

1 **Temperature-enhanced effects of iron on Southern Ocean phytoplankton**

2

3 Charlotte Eich^{†,1,2,*}, Mathijs van Manen^{†,3}, J. Scott P. McCain^{4,5}, Loay J. Jabre^{4,6}, Willem H. v.d. Poll⁷, Jinyoung
4 Jung⁸, Sven B. E. H. Pont¹, Hung-An Tian³, Indah Ardiningsih³, Gert-Jan Reichart^{3,9}, Erin M. Bertrand⁴, Corina
5 P.D. Brussaard^{1,2,*}, Rob Middag^{3, 10}

6

7 [†]These authors contributed equally to this work.

8 Affiliations:

9 ¹Department of Marine Microbiology and Biogeochemistry, NIOZ Royal Netherlands Institute for Sea Research,
10 1797 SZ 't Horntje, The Netherlands

11 ²Institute for Biodiversity and Ecosystem Dynamics (IBED), University of Amsterdam, 1098 XH Amsterdam,
12 The Netherlands

13 ³Department of Ocean Systems, NIOZ Royal Netherlands Institute for Sea Research, 1797 SZ 't Horntje, The
14 Netherlands

15 ⁴Department of Biology, Dalhousie University, Halifax, Nova Scotia, Canada

16 ⁵Current Address: Department of Biology and Department of Earth, Atmospheric, and Planetary Sciences,
17 Massachusetts Institute of Technology, Cambridge, MA 02142, USA

18 ⁶Current Address: Marine Chemistry & Geochemistry Department, Woods Hole Oceanographic Institution,
19 Woods Hole, MA 02543, USA

20 ⁷CIO Oceans, Energy and Sustainability Research Institute Groningen, Faculty of Science and Engineering,
21 University of Groningen, Nijenborgh 7, Groningen, AG 9747, The Netherlands.

22 ⁸Korea Polar Research Institute, 26, Songdomirae-ro, Yeonsu-gu, Incheon 21990, Republic of Korea

23 ⁹Department of Earth Sciences, Faculty of Geosciences, Utrecht University, Utrecht, the Netherlands

24 ¹⁰Centre for Isotope Research-Oceans, Energy and Sustainability Research Institute Groningen, Faculty of Science
25 and Engineering, University of Groningen, 9712 CP Groningen, The Netherlands

26

27 *Correspondence to: Charlotte Eich (charlotte.eich@nioz.nl) & Corina Brussaard (corina.brussaard@nioz.nl)

28

29 **Short summary**

30 Phytoplankton growth in the Southern Ocean (SO) is often limited by low iron (Fe) concentrations. Sea surface
31 warming impacts Fe availability and can affect phytoplankton growth. We used Fe clean shipboard incubations
32 to test how changes in Fe and temperature affect SO phytoplankton. Their abundances usually increased with Fe
33 addition and temperature increase, with Fe being the major factor. These findings imply potential shifts in
34 ecosystem structure, impacting food webs and elemental cycling.

35

36 **Abstract**

37 Iron (Fe) is a key limiting nutrient for Southern Ocean phytoplankton. Input of Fe into the Southern Ocean is
38 projected to change due to global warming, yet the combined effects of a concurrent increase in temperature with
39 dissolved Fe (dFe) addition on phytoplankton growth and community composition are understudied. To improve
40 our understanding of how Antarctic phytoplankton communities respond to Fe and enhanced temperature, we
41 performed four full factorial onboard bioassays under trace metal clean conditions with phytoplankton
42 communities from different regions of the Weddell and the Amundsen Seas in the Southern Ocean. Treatments
43 consisted of a combined 2 nM Fe addition with 2 °C warming treatment (TF), compared to the single factor
44 treatments of Fe addition at *in-situ* temperature (F), and non-Fe addition at + 2 °C (T) and at *in-situ* temperature
45 (C). Temperature had limited effect by itself but boosted the positive response of the phytoplankton to Fe addition.
46 Photosynthetic efficiency, phytoplankton abundances, and chlorophyll *a* concentrations typically increased
47 (significantly) with Fe addition (F and/or TF treatments) and the phytoplankton community generally shifted from
48 haptophytes to diatoms upon Fe addition. The < 20 µm phytoplankton fraction displayed population-specific
49 growth responses, resulting in a pronounced shift in community composition and size distribution (mainly towards
50 larger-sized phytoplankton) for the F and TF treatment. Such distinct enhanced impact of dFe supply with
51 warming on Antarctic phytoplankton size, growth and composition will likely affect trophic transfer efficiency
52 and ecosystem structure, with potential significance for the biological carbon pump.

53

54 Keywords: Antarctic algae, bioassays, size-fractionation, climate change, trace metals

55 **1. Introduction**

56 The Southern Ocean plays an important role in regulating the Earth's climate as it is an important sink for CO₂
57 (Takahashi et al., 2012; Friedlingstein et al., 2022; Fisher et al., 2023). Phytoplankton take up CO₂ and convert it
58 to biomass, forming not only the base of the pelagic food web but also driving the biological carbon pump
59 (Buesseler et al., 2020; Huang et al., 2023). During the short austral productive season, however, Antarctic
60 phytoplankton growth often becomes limited by low iron (Fe) availability (e.g., Martin et al., 1990; Boyd, 2002;
61 Ryan-Keogh et al., 2023). Fe is a vital micronutrient for a variety of cellular processes, including photosynthesis
62 (Geider & La Roche, 1994; Schoffman et al., 2016; Kroh & Pilon, 2020) and nitrate assimilation (Schoffman et
63 al., 2016, Milligan and Harrison, 2000). Shortage of Fe results in so called high nutrient, low chlorophyll (HNLC)
64 conditions, where the ratio of macronutrients, especially nitrate, relative to total Chlorophyll *a* (Chl *a*)
65 concentrations is comparably high (Minas & Minas, 1992; Sarmiento et al., 2004; Venables & Moore, 2010;
66 Basterretxea et al., 2023).

67 Trace metal supply in the Southern Ocean follows a strong seasonal cycle where in winter Fe is replenished via
68 deep water-mixing (Tagliabue et al., 2014) or sediment resuspension in coastal areas (Boyd et al., 2012), to be
69 quickly depleted again by phytoplankton uptake in the next season. Predicted increases in stratification may
70 weaken Fe supply to surface waters from below (Sallée et al. 2011), however, this is still uncertain as increased
71 stratification might not have a strong effect or might even increase turbulent nutrient fluxes associated with
72 breaking internal waves (van Haren et al., 2020). Additionally, increased stratification effects may be counteracted
73 by a deepening of mixed layer depths (Sallée et al., 2021) and changes in gyre-scale circulations (Misumi et al.,
74 2013). In general, Fe limitation for Antarctic phytoplankton is predicted to be at least partially relieved in the
75 future (Bazzani et al., 2023) because of enhanced Fe supply by increased wind driven mixing (due to reduced ice-
76 induced stratification) and sources associated with ice melt, i.e., glaciers (Annett et al., 2015; Sherrell et al., 2015;
77 Van der Merwe et al., 2019; Seyitmuhammedov et al., 2022, Moreau et al. 2023) icebergs (Raiswell et al., 2008;
78 Shaw et al., 2011; Raiswell et al., 2016; Hopwood et al., 2019) or sea-ice (Lannuzel et al., 2016; Gerringa et al.,
79 2020). In the Amundsen Sea, increased Fe input is likely to occur due to enhanced glacial melt and runoff,
80 particularly during the summer months when melting is most pronounced (e. g., Van Manen et al., 2022). Increases
81 in seawater temperature may affect the availability of Fe for phytoplankton, since temperature affects the oxidation
82 of the bioavailable Fe(II) to Fe(III) (e.g., Millero et al., 1987), however, Aflenzer et al. (2023) did not observe a
83 lower bioavailability of added Fe with increased temperatures. In the Weddell Sea, Fe input may increase through
84 upwelling of Fe-rich deep waters and meltwater from ice shelves, but this is less certain (Klunder et al., 2011).

85 Seasonal variations in sea ice cover and glacial melt will play a significant role in determining the timing and
86 magnitude of Fe input in these regions. These changes in Fe supply are associated with ongoing climate change
87 that is projected to lead to elevated temperatures and changes in wind patterns as well as associated currents and
88 upwelling (Turner et al., 2005; Moore et al., 2018). Overall, future Southern Ocean conditions will most likely be
89 warmer with potentially elevated Fe concentrations, which can be expected to also affect phytoplankton
90 productivity and community composition (Boyd et al., 2015; Laufkötter et al., 2015, Pinkerton et al., 2021).
91 Depending on the geographical region and the time in the productive season (Thomalla et al., 2023), global
92 warming is predicted to increase wind-induced mixing or strengthen vertical stratification (Bronse laer et al., 2020;
93 De Lavergne et al., 2014; Hillenbrand & Cortese, 2006; Shi et al., 2020). Phytoplankton will bloom earlier in the
94 productive season as a result of decreasing sea ice and consequently higher light (Krumhardt et al., 2022), most
95 likely rapidly drawing down available Fe followed by stratification, and thus favourable conditions for smaller-
96 sized phytoplankton (Deppeler & Davidson, 2017; Krumhardt et al., 2022). Besides Fe and temperature, there are
97 also other factors, e.g., other bio-essential metals (Mn, Co, Ni, Cu and Zn), where notably Mn has been shown to
98 be (co-)limiting in the Southern Ocean (Wu et al.; 2019, Browning et al., 2021, Balaguer et al.; 2022, Hawco et
99 al.; 2022). Mn is essential for phytoplankton photosystems (Raven et al., 1990) and a co-factor for enzymes
100 dealing with oxidative stress (Wolfe-Simon et al., 2005). Moreover, light is another major limiting factor for
101 phytoplankton growth in Southern Ocean (e.g., van Oijen et al.; 2004, Strzepek et al.; 2019, Vives et al.; 2022,
102 Latour et al.; 2024).

103 Considering the urgency of warming and the anticipated change in Fe supply, there is a need for studies
104 investigating the combined effects of these two important drivers controlling phytoplankton growth in the
105 Southern Ocean. There are many reports on the effects of Fe addition to Fe-limited phytoplankton from the
106 Southern Ocean (Reviewed by e.g., Yoon et al., 2018; Bazzani et al., 2023) and several on the influence of
107 temperature (Reay et al., 2001; Morán et al., 2006; Boyd et al., 2013), but only few studies examined the combined
108 effects of Fe and temperature on Antarctic phytoplankton (i.e. Rose et al., 2009; Zhu et al., 2016; Andrew et al.,
109 2019; Jabre & Bertrand, 2020; Jabre et al., 2021; Aflenzer et al., 2023). In particular, studies using natural
110 phytoplankton communities are scarce (Rose et al., 2009; Jabre et al., 2021) and concentrated on Ross Sea
111 phytoplankton with relatively large temperature increases (3 to 6 °C). Hence, more insight into how phytoplankton
112 from other regional Antarctic seas respond to the warming projected by the year ~2100 (Meredith et al., 2019) is
113 needed.

114 The Weddell Sea is one of the key areas of dense Antarctic bottom water formation (Fahrbach et al., 2004) and
115 plays an important role in the global thermohaline circulation. The subpolar cyclonic Weddell Gyre circulating in
116 the Weddell Sea basin isolates the centre of the Weddell Sea from marginal Fe sources such as melt or sediments,
117 whilst the currents on the edges of the gyre have the potential to pick up Fe from a variety of sources, such as the
118 seafloor, bathymetry driven mixing with deeper water masses, and sources associated with ice melt (Klunder et
119 al., 2014; Sieber et al., 2021, Tian et al., in prep.). Generally, the Weddell Sea has a relatively low primary
120 productivity, associated with Fe limitation in the centre of gyre (Hoppema et al., 2007; Klunder et al., 2014). In
121 contrast, the west Amundsen Sea and specifically the Amundsen Sea Polynya (ASP) is known as one of the most
122 productive regions in the Southern Ocean in terms of net primary production per net area (Arrigo & van Dijken,
123 2003). Additionally, this region (ASP) is characterised by a fast thinning of ice-sheets, shelf ice and glaciers, with
124 associated input of Fe required to sustain the high levels of primary productivity (e.g., Gerringa et al., 2012; van
125 Manen et al., 2022). Nevertheless, phytoplankton in the ASP could still be stimulated by additional Fe input
126 (Alderkamp et al., 2015).

127 The aim of the current study is to examine the concurrent effects of Fe supply and warming on Antarctic
128 phytoplankton communities from the Weddell Sea and the Amundsen Sea under controlled trace metal clean
129 conditions. Given the naturally low dissolved Fe (dFe) concentrations in the Southern Ocean, trace metal clean
130 conditions are crucial to avoid confounding Fe effects when studying temperature alone (Middag et al., 2023).
131 Our bioassay treatments comprised a full factorial combination of dFe and temperature increases. The temperature
132 was enhanced by 2 °C, based on forecasts from the IPCC report (Meredith et al., 2019). Whilst the Amundsen Sea
133 has shown a warming trend over the past years already (Gómez-Valdivia et al., 2023; Drijfhout et al., 2024), the
134 surface waters of the Weddell Sea have not (yet) shown a clear increasing temperature trend, but underlying waters
135 are warming (Strass et al., 2020), and local temperature increases due to upwelling of warm deep water have been
136 observed (Darelius et al., 2023; Teske et al., 2024). The concentration of dFe in the Fe addition treatments (F and
137 TF) was increased by 2 nM. Future Fe concentrations are highly uncertain (Hutchins & Boyd, 2016; Tagliabue et
138 al., 2016; Ryan-Keogh et al., 2023), and not necessarily linked to bioavailability of Fe (Van Manen et al., 2022;
139 Fourquez et al., 2023), but previous experiments in the Southern Ocean have shown that such an addition
140 represents (temporarily) Fe replete conditions (De Baar et al., 2005). Moreover, increased Fe availability in the
141 Southern Ocean could have a far-reaching impact, leading to increased nutrient consumption consequently
142 reducing nutrient transfer to lower latitudes where primary production is fuelled by these nutrients (Primeau et
143 al., 2013; Moore et al., 2018). By integrating biological and trace metal chemistry analyses within large volume

144 (20 L cubitainers), trace metal clean experiments, we aim to provide a clearer understanding of future changes in
145 phytoplankton growth patterns and the implications for the Southern Ocean's role in global climate regulation.

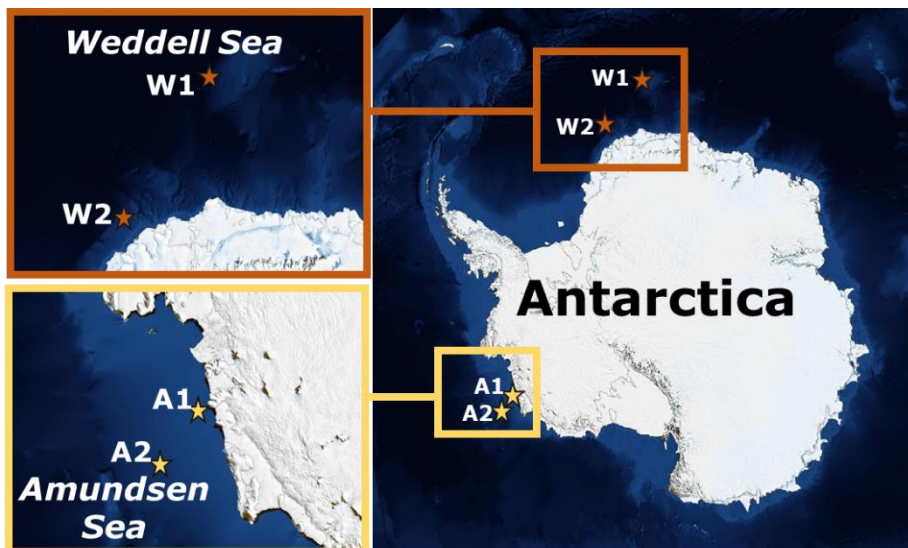
146

147 2. Material and Methods

148 2.1 Location and sampling

149 Natural seawater for the bioassays was collected during research expeditions (Fig. 1) in the Amundsen Sea
150 (bioassays A1 and A2, R/V Araon, ANA08B, 2017/18) and in the Weddell Sea (bioassays W1 and W2, R/V
151 Polarstern (Alfred-Wegener-Institut Helmholtz-Zentrum für Polar- und Meeresforschung 2017), PS117, 2018/19)
152 in austral summer (December – February).

153



154

155 **Figure 1:** Location of the four bioassay experiments: Bioassays A1 and A2 were performed in the Amundsen Sea and W1 and
156 W2 in the Weddell Sea (Image obtained from NASA Worldview).

157

158 Seawater was sampled at the autofluorescence maximum (36 m for A2 and 20 m for both W1 and W2), except
159 for bioassay A1, which did not show an autofluorescence maximum and was sampled at the mid-mixed layer
160 depth (15 m). Water for each bioassay was collected in a single deployment of NIOZ's Titan ultraclean CTD
161 sampling system for trace metals (De Baar et al., 2008), mounted with pristine large volume samplers (Rijkenberg
162 et al., 2015). To prevent light shock for the phytoplankton, the original Polyvinylidene fluoride (PVDF) Pristine
163 samplers were replaced by a light-proof poly-propylene version. Salinity (conductivity), temperature,
164 fluorescence, depth (pressure) and oxygen were measured with a CTD (Seabird SBE 911+) mounted on the trace
165 metal clean sampling system (De Baar et al., 2008). To avoid contamination, further processing was performed

166 under trace metal clean, dimmed light conditions and at 2 °C in a cleanroom environment inside a modified high-
167 cube shipping container which fits the Titan sampling system. During transport on deck, cubitainers were covered
168 with black light-proof bags to avoid light stress.

169 Water for Amundsen Sea bioassay A1 was sampled from the middle of the ASP and for bioassays A2 in the
170 marginal sea ice zone just outside of the ASP. Both W1 and W2 were performed with water from the eastern
171 Weddell Sea. The Amundsen Sea bioassays A1 and A2 ran for 6 days (25 to 31 January and 31 January to 6
172 February 2018, respectively), whilst the Weddell Sea bioassays W1 and W2 ran for 8 days (28 December 2018 to
173 5 January and 9 to 17 January 2019, respectively, see Fig. S1 for regional Chlorophyll *a* concentrations at the start
174 of bioassay incubations and Fig. S2 for station depth profiles). Amundsen Sea bioassays were thus initiated
175 towards the end of the reported bloom period (Arrigo et al. 2012), whilst Weddell Sea bioassays were initiated
176 during the start of the bloom period (von Berg et al., 2020).

177 **2.2 Bioassay incubation set-up**

178 Incubations were performed in custom built deck incubators (see Supplement Bioassay Setup for more
179 information). Collapsible 20 L cubitainers (LDPE with PP caps and fitted with PE faucet; Cole-Palmer, Illinois,
180 USA) were used. These were soap and HCL (1 M) cleaned prior to the expeditions and stored with full surface
181 contact in 0.024 M HCl (VWR Normatom Ultrapur, Avantor, Radnor, USA) for at least two months. Before use,
182 cubitainers were rinsed five times with ambient seawater. The natural seawater for the actual incubations was
183 distributed randomly to the total of 12 cubitainers which were then randomly assigned to the different treatments.
184 Trace metal clean conditions were maintained during all sampling and sample handling.

185 The bioassay treatments (performed in triplicate) were: *in-situ* conditions (control, C), + 2 nM dFe (as FeCl₃)
186 addition (F), + 2 °C temperature increase (T), and + 2 nM dFe addition and + 2 °C temperature increase (TF). For
187 the Amundsen Sea bioassays, a natural isotopic composition (natural dFe) was used for the dFe addition, whilst
188 d⁵⁷Fe was used in the Weddell Sea bioassays. This practice was adopted to better differentiate the added Fe from
189 the naturally present Fe, as we noticed that the dFe concentration in Fe amended Amundsen Sea bioassays quickly
190 returned to background concentrations (see section 3.1). Measuring Fe with a natural isotopic composition at these
191 low concentrations is still a challenge and combined with inherent variability between replicates. After several
192 days it became impossible to distinguish the Fe amended and non-amended treatments in Amundsen Sea bioassays
193 based on their natural dFe concentration (see section 3.1). The variation in natural dFe expected between Fe
194 amended and non-amended treatments despite precipitation and uptake, was hidden in the analytical and
195 environmental variability. For Weddell Sea bioassays we thus decided to add ⁵⁷Fe, a rare (2.12 % abundant vs

196 91.75 % for ^{56}Fe) natural isotope of Fe. Given its low natural abundance, ^{57}Fe is not nearly as sensitive to analytical
197 and replicate variation as such variation is insignificant relative to the addition, allowing better insight in Fe
198 drawdown over the course of the experiments.

199 Average starting concentrations of dFe in the Fe addition treatments ranged from 2.03 to 2.28 nM for both Weddell
200 and Amundsen Sea bioassays. Temperatures in the T and TF treatments were 1.4, 0.4, 1.7 °C and 1 °C, for A1,
201 A2, W1 and W2, respectively (see Table 1 for an overview of starting conditions in all treatments). One replicate
202 of the control treatment in bioassay W1 started leaking during the incubation and was thus not sampled from day
203 4 onwards. For bioassay W2, the *in-situ* temperature of -1.4 °C could not be maintained due to the very sunny
204 weather, resulting in an increase of 0.4°C for all treatments. Final incubation temperatures were -1.0 °C in the
205 control (C) and Fe-only (F) treatment and 1 °C (instead of 0.6 °C) in the T and TF treatments. This temperature
206 adjustment was done slowly over the course of 24 h on the second day of the incubation. More details about the
207 set-up can be found in the supplemental data (Fig. S3, supplement Bioassay Setup). Over the course of the
208 incubation period, temperatures were kept constant, with a maximum temperature fluctuation of ± 0.3 °C.

209 For Amundsen Sea bioassays, light levels were chosen to mimic *in-situ* conditions, but noting the low light
210 conditions during these incubations (ca. 3 % of in-air photoactive radiation, PAR; i.e. average 3.4 and 1.5 μmol
211 $\text{quanta m}^{-2} \text{s}^{-1}$ for A1 and A2 over the course of incubation), we opted for non-limiting light conditions (Bertrand
212 et al., 2011) for the (later performed) bioassays of the Weddell Sea (ca. 12 % of in-air PAR; i.e. average 69 and
213 100 $\mu\text{mol quanta m}^{-2} \text{s}^{-1}$ for W1 and W2 over the course of incubation). The percentages and values reported refer
214 to approximate light conditions within cubitainers. Light levels were adapted using neutral density screens.
215 Samples for dissolved and particulate metals, Chl *a*, pigment-based taxonomic analyses, and particulate organic
216 carbon (POC), nitrogen (PON) and phosphate (POP) were taken before filling of the cubitainers at the start of the
217 bioassay incubations (t_0), and at the end of the incubations after 6 (Amundsen Sea) or 8 (Weddell Sea) days
218 (difference in duration due to logistical constraints). Samples for phytoplankton photosynthetic efficiency (F_v/F_m)
219 and phytoplankton abundances were taken at least every other day. Macronutrients were measured on board at
220 least every other day to screen for potential macronutrient limitation.

221

222 **2.3 Setup verification**

223 To test for potential Fe contamination, three cubitainers were filled with ultrapure (UP) water and handled and
224 subsampled using the same methods and frequency as the treatments. Subsamples for dFe analysis were taken at
225 the start (0.08 ± 0.04 nM) and after three (0.07 ± 0.04 nM) and six (0.06 ± 0.04 nM) days. Concentrations of dFe

226 stayed consistently low, suggesting minimal or no contamination. We also tested whether added dFe stayed in
227 solution or adsorbed to the cubitainer walls and found a slow gradual decrease over the first few days in dFe
228 concentrations after addition to UP water that we attribute to precipitation and wall adsorption (Table S1). During
229 our experiments, the concentrations of added dFe decreased more rapidly, whereas the dFe concentrations in the
230 non-Fe treatments, as well as the non-added form of dFe in Fe treatments ($d^{57}\text{Fe}$ for Amundsen and natural dFe
231 for Weddell Sea bioassays), stayed low and relatively constant over time. Since phytoplankton grew in all
232 treatments, the faster decrease of added dFe was likely due to uptake and sorption onto (biogenic) particles rather
233 than precipitation to the cubitainer walls. Low traceable amounts of $d^{57}\text{Fe}$ during the second half of the incubations
234 in W1 and W2 suggested that the initial decrease in dFe concentrations did not correspond to permanent removal
235 from the bioavailable Fe pool (e.g., due to absorption; Jensen et al., 2020) but instead buffered the dissolved pool
236 (as suggested for natural settings with exchange between the (labile) pFe and dFe pools; Van Manen et al., 2022),
237 or that most of the added dFe was taken up by phytoplankton as rapid luxury uptake during the first days of an
238 experiment (Lampe et al., 2018).

239

240 **2.4 Macronutrients**

241 During the Amundsen Sea bioassays, dissolved macronutrients were measured onboard following Jeon et al.
242 (2021), according to the Joint Global Ocean Flux Study (JGOFS) protocols (Gordon et al., 1993) using a four-
243 channel Auto-Analyzer (QuAatro, Seal Analytical, Norderstedt, Germany). Measurement precisions were ± 0.02 ,
244 ± 0.28 and $\pm 0.14 \mu\text{M}$ for phosphate, silicate, and nitrogen (nitrate + nitrite), respectively (Jeon et al., 2021). For
245 Weddell Sea bioassays, samples for nitrate, nitrite, phosphate, and silicate were measured following the method
246 described by Gerringa et al. (2019). Measurements precisions were ± 0.01 , ± 0.31 and $\pm 0.04 \mu\text{M}$ for phosphate,
247 silicate, and nitrogen (nitrate + nitrite), respectively.

248

249 **2.5 Dissolved and particulate metals**

250 Cubitainers were subsampled for dFe as well as other dissolved trace metals (dMn, dCo, dCu, dNi, dZn, dCd)
251 using a $0.2 \mu\text{m}$ Sartobron-300 filter cartridge (Sartorius AG, Göttingen, DE) for bioassay A1 and A2 and pre-acid
252 cleaned $0.2 \mu\text{m}$ Acropak filter cartridges (Cytiva, Marlborough, USA) for W1 and W2. Filters were fitted to an
253 UP-cleaned vented PE faucet attached to the cubitainer with HCl acid (1.5 M) cleaned silicon tubing. Filtered
254 samples were taken by applying pressure to the cubitainer. Different filters were used for Fe replete and deplete
255 treatments, and filters were replaced between experiments. The dissolved trace metal samples were collected in

256 acid cleaned 125 mL LDPE bottles following GEOTRACES protocols (Cutter et al., 2017) and directly acidified
257 by adding ultra-pure HCl (Baseline®HCl; Seastar Chemicals Inc, Sidney, CA), resulting in a concentration of
258 0.024 M with a final pH of ~1.8. Samples were stored until analysis at NIOZ. Trace metal samples were prepared
259 and analysed following van Manen et al. (2022) and references within. In short, trace metal samples were
260 pre-concentrated using a SeaFAST pre-concentration system (ESI). Blank contributions from sample handling,
261 pre-concentration, and analysis steps were determined by analysing acidified MQ water (~1.8 pH) prepared in the
262 same way as real samples.

263 For particulate trace metals (pFe, pMn, pCo, pCu, pZn, pCd, pAl) and POP, 25 mm poly-ether-sulfone (PES) disc
264 filters (0.45 µm Pall Supor, Port Washington, USA) and polypropylene filter holders (Advantec, Cole-Parmer,
265 Vernon Hills, USA) were used, following the protocol adapted by Van Manen et al. (2022) with one additional
266 step: samples were soaked for at least 30 minutes in oxalate-EDTA (respectively 0.75M and 5.5M) in a 10L carboy
267 (VWR Collection; Avantor, Radnor, USA) to remove all trace metals outside or adsorbed to phytoplankton cell
268 walls (modified after Hassler & Schoemann, 2009) and subsequently filtered. The EDTA oxalic acid wash used
269 on particulate samples prior to filtration should effectively remove surface-bound metals, also minimizing the
270 authigenic Fe fraction. Due to time limitations, samples for particulate metals were only taken during experiment
271 A1, W1 and W2. After filtration, which happened at the end of the experiments, filters were stored frozen at -20
272 °C until analysis. In the NIOZ lab, filters were treated with two successive digestion steps to determine the total
273 particulate fraction. All vials used in the digestion procedures were rigorously cleaned with HF and HCl
274 beforehand and rinsed with UP water. Filters were subjected to a leach consisting of 1.8 mL of 4.35M (25 %) two
275 times sub-boiled distilled acetic acid and 0.02M (2 %) hydroxylamine hydrochloride (99.999 % trace metal basis,
276 Sigma-Aldrich, Saint-Louis, USA). Subsequently, filters were digested following the total digestion protocol
277 developed by Cullen & Sherrell (1999) and modified by Planquette & Sherrell (2012). A volume of 2 mL of 3 ×
278 sub-boiled distilled 8.0 M (50 %) HNO₃ (VWR Chemicals – AnalaR NORMAPUR, Avantor, Radnor, USA) and
279 2.9 M (10 %) HF (Merck – Supelco, Kenilworth, USA) was added. The vials were closed tightly and refluxed for
280 4 h at 110 °C. The solution was then transferred to a secondary Teflon vial and were then heated to near dryness
281 at 110 °C. A 1 mL volume of 8.0 M (50 %) 3× sub-boiled distilled HNO₃ (VWR Chemicals– AnalaR
282 NORMAPUR, Avantor, Radnor, USA) and 15 % H₂O₂ (Merck – Suprapur, Kenilworth, USA) was added to the
283 dried vial contents. The vials were refluxed for 1 h at 110 °C and subsequently cooled to room temperature.
284 Addition of reagents and refluxing were repeated once. After this repetition, the vials were heated to near dryness

285 at 110 °C. The samples were re-dissolved in 2 mL 1.5 % 3× sub-boiled distilled HNO₃ with 10 ppb Rh as internal
286 standard and transferred to 2 mL Cryovials® (VWR, Avantor, Radnor, USA) for storage and analysis.

287 The lithogenic fraction and concentration of pFe and other particulate metals discussed was determined by
288 assessing the ratio between the particulate metal of interest and particulate aluminium (pAl), assuming all pAl
289 originates from crustal material using the approach described in more detail in van Manen et al (2022). For
290 example, we are using the observed pFe/pAl ratio in the samples and the known crustal ratio of 0.21 mol mol⁻¹
291 (Taylor and McLennan, 1985) to calculate the lithogenic pFe fraction and concentration.

292

293 **2.6 ICP-MS trace metal measurements and particulate organic phosphorous**

294 Dissolved trace metal samples were preconcentrated using a SeaFAST pre-concentration system (ESI) using two
295 loops of 10 mL and were eluted into 350 µL elution acid (1.5 M Teflon distilled HNO₃ with rhodium as internal
296 standard) which gives a pre-concentration factor of 57.14 (see van Manen et al., 2022). Dissolved trace metal
297 samples, blanks (Table S2), and references (Table S3) were analysed by ICP-MS (Thermo Scientific Sector Field
298 High-Resolution Element 2, Thermo Fisher-Scientific, Waltham, USA). Blank values were much lower than the
299 analysed samples, and reference results were in good agreement with certified values.

300 For the particulate samples, including POP, the procedure blanks without a filter were treated identically to the
301 samples, except for the steps involving filter handling and the removing of the filter from the filter holders.
302 Therefore, the vial blank is included in this reagent blank. Filter blanks consisted of unused acid cleaned PES disc
303 filters (Table S4).

304 Accuracy and precision of the digestions were assessed by Certified Reference Materials (CRMs). There is no
305 CRM available for marine suspended particulate matter, therefore accuracy could only be approximated by
306 analysis of other available CRMs. PACS-2 and MESS-3 (marine sediments, National Research Council of
307 Canada) were analysed. For each CRM, 10-30 mg were digested, whilst recommended sample weights are 250
308 mg for PACS-2 and MESS-3. The lower sample weights in this study were chosen to be representative of actual
309 marine particulate suspended matter concentrations (similar to Ohnemus et al., 2014). PACS-2 and MESS-3 were
310 only subjected to the total digestion (Table S5). The CRMs were in good agreement with the certified values.

311

312 **2.7 Particulate organic carbon and nitrogen**

313 For POC and PON sampling, 1 L of unfiltered seawater was collected from each cubitainer and stored in dark
314 bottles (Nalgene, Rochester, USA) at 1 °C until further processing (within 4 h after sampling). Filtrations were

315 then performed using combusted (4 h at 500 °C; Verardo et al., 1990) 0.3 µm 25 mm GF75 filters (Whatman,
316 Cytiva, Maidstone UK) and under modest under pressure (max. 200 mbar). Filters were folded once, packed in
317 aluminium foil, and stored frozen (-20 °C) until analysis. The POC and PON concentrations were measured using
318 a Thermo-Interscience Flash EA1112 Series Elemental Analyzer (Thermo Scientific, Waltham, USA) with excess
319 oxygen, at 900 °C and a detection limit of 100 ppm and a precision of 0.3 % (Verardo et al., 1990). Before analysis,
320 GF75 filters were folded and packed into a tin cup. The instrument blank is included by the analyser calibration.
321 Carbon and nitrogen content of samples and blanks were computed according to the results of the standard
322 measurements, and the blank was subtracted from the sample. Acetanilide (C₈H₉NO) with 71.09 % C and 10.36
323 % N (ThermoQuest, Milan, Italy) was measured as standard material, and silty and sandy soil standards from
324 Elemental Microanalysis were measured as an internal reference.

325

326 **2.8 Phytoplankton photosynthetic efficiency**

327 F_v/F_m was determined in a Water-K quartz cuvette (3.5 mL) using pulse amplitude modulated fluorometry (Heinz
328 Walz WATER-PAM, with Red LEDWATER-ED cuvette version S/N EDEE0196, Walz GmbH, Effeltrich,
329 Germany). Samples were kept in 50 mL Greiner tubes (Thermo Fisher-Scientific, Waltham, USA) in the cold
330 (stored in a cool box on ice) and in the dark for dark-adaptation (15 min up to occasionally 4 h). Acclimation
331 times of up to 4 h did not affect photosynthetic efficiency of different phytoplankton (L. Peperzak, personal
332 communication; Eich et al., 2021). The measuring light frequency used was set to level 5 (25 Hz) with an intensity
333 of 8, the SAT-pulse width was set to 0.8 seconds and the far-red pulse width was set to 10 seconds, with intensities
334 of 10 and 6, each. The cuvette was rinsed with ultra-pure (UP) water between samples, which was removed by
335 shaking the cuvette and placing it upside down on lint-free paper towels to remove any remaining droplets (testing
336 technical replicates did not show a significant effect of UP rinsing, non-parametric Kruskal-Wallis ANOVA, $p =$
337 0.95). The relative fluorescence yield (F_t) values were kept between 100 and 1000 by adjusting the PM-gain.
338 Blanking was done for each station and/or bioassay using 0.2 µm filtered seawater (Cullen & Davis 2003) from
339 the respective stations and repeated after PM-gain adjustment when needed. The following formula was used to
340 obtain the photosynthetic efficiency: $F_v/F_m = (F_m - F_0)/F_m$, with F_0 being the minimum fluorescence, and F_m being
341 the maximum fluorescence.

342

343 **2.9 Chlorophyll a concentration and pigment-based taxonomic analyses**

344 Samples (0.54 - 2.65 L) for Chl *a* concentrations and pigment-based community composition were filtered within
345 30 min of subsampling (kept on ice and in the dark) on GF/F glass fibre filters (25 mm diameter, Whatman,
346 Cytiva, Marlborough, USA) using a vacuum pump (max. 200 mbar), until filters showed clear colouring. Samples
347 were taken for total as well as a < 20 µm fraction for better compatibility with phytoplankton community
348 measurements by flow cytometry. For the < 20 µm fraction, natural seawater was reverse sieved through a 20 µm
349 mesh before filtration onto a GF/F filter. Due to low sample volume availability at bioassay A2, the same amount
350 of water from all replicates was combined for both total and < 20 µm Chl *a* samples, resulting in one averaged
351 value for each treatment. Filters were folded once and double wrapped in aluminium foil, flash-frozen in liquid
352 nitrogen and stored at -80 °C until further analysis in the home lab. Pigments were dissolved in 90 % acetone from
353 the freeze-dried filters according to Van Leeuwe et al. (2006) and high-performance liquid chromatography
354 (HPLC) pigment separation was performed (Zobrax-Eclipse XDB-C8 column, 3.5 µm particle size) according to
355 Van Heukelem & Thomas (2001). Detection of pigments was based on both the retention time and diode array
356 spectroscopy of standards (346 nm, Waters 996), quantification was based on calibration curves using those
357 standards (DHI LAB standards). Phytoplankton community composition was determined using CHEMTAX
358 version 1.95 (Mackey et al., 1996), following Selz et al. (2018). For the final pigment ratios, see Table S6.

359

360 **2.10 Phytoplankton and bacterial abundances (< 20 µm)**

361 Phytoplankton cell abundances (< 20 µm) were obtained using a 488 nm Argon laser benchtop Beckton-Dickinson
362 FACSCalibur (BD Biosciences, Franklin Lakes, USA) flow cytometer with the trigger set on red Chl *a*
363 autofluorescence (Marie et al., 1999). The phytoplankton samples from the Amundsen Sea bioassays were
364 measured fresh within 30 min of sampling (stored on ice); the Weddell Sea bioassay phytoplankton samples were
365 fixed for 15 – 30 min with 100 µL formaldehyde-hexamine (18 % v/v:10 % v/v) at 4 °C, flash-frozen in liquid
366 nitrogen and stored at -80 °C until analysis in the home lab. Phytoplankton populations were differentiated based
367 on their red autofluorescence and side scatter, using FCS express 5 (De Novo Software, Pasadena, CA, USA).
368 Freshly counted samples resulted in comparable gating as the fixed samples (tested for Amundsen Sea samples).
369 A total of 25 populations were distinguished (Table S7), whereby not all populations occurred in both seas and
370 all bioassays. Average cell diameters were determined by size-fractionation, i.e., serial gravity filtration through
371 20, 10, 8, 5, 3, 2, 1, 0.8 and 0.6 µm PC filters (Whatman, Cytiva, USA, Marlborough, MA) using a reuseable filter

372 holder (Whatman, Cytiva, Marlborough, USA) and a plastic syringe. The number of cells retained by each filter
373 per discriminated population were plotted against the respective filter size. The average cell diameters were
374 defined as the size where 50 % of the original number of cells were retained, based on the fit of a sigmoidal plot
375 (Veldhuis & Kraay, 2004). Phyto 5, 6, 7, 11, 12 and 14 were cryptophytes that were identified by their orange
376 phycoerythrin autofluorescence. Based on earlier work (Biggs et al., 2019), we consider phytoplankton
377 populations Phyto 20 and 22 to 25 to be diatoms and Phyto 8 to be *Phaeocystis antarctica* by comparing the red
378 autofluorescence and side scatter pattern of the respective phytoplankton groups. The latter was confirmed during
379 the Amundsen Sea expedition when we selectively collected *Phaeocystis* colonies and analysed them fresh
380 onboard after gentle shaking (to break up the colonies). Phytoplankton carbon was estimated based on cell volume
381 of phytoplankton, assuming spherical cells, and using $237 \text{ fg C } \mu\text{m}^{-3}$ for picophytoplankton populations Phyto 1
382 to 6 and $196.5 \text{ fg C } \mu\text{m}^{-3}$ for nanophytoplankton populations Phyto 7 to 25 (Garrison et al., 2000; Worden et al.,
383 2004). Phytoplankton net growth rates were calculated using exponential trendlines. For total abundances, the full
384 incubation period was taken into account (i.e., day 1 - 6 for Amundsen Sea and day 2 - 8 for Weddell Sea
385 bioassays). Starting abundances were taken prior to filling of the cubitainers and hence not taken into account.
386 For the phytoplankton group specific rates only those time points (>3 but most often 4-5 time points) with a
387 consecutive increase in abundances were selected.

388 Samples for bacterial abundances were fixed with EM-grade glutaraldehyde (0.5% final concentration; Sigma-
389 Aldrich, Zwijndrecht, The Netherlands), flash-frozen in liquid nitrogen and stored at -80°C until analysis using
390 flow cytometry (Marie et al.; 1999). Bacterial carbon concentrations were calculated assuming $12.4 \text{ fg C cell}^{-1}$
391 (Fukuda et al.; 1998).

392

393 **2.11 Statistical analyses**

394 All statistical analyses were performed using R (R Core Team, 2021). To detect differences in phytoplankton
395 community composition between treatments, an ANOSIM analysis was performed (vegan library, using Bray-
396 Curtis dissimilarity with 9999 permutations). When a significant difference ($p < 0.05$) was detected, an indicator
397 species analysis (vegan library, function `r.g.` with 9999 permutations) was used as a follow-up analysis to see
398 which phytoplankton groups differed between treatments. This was done for both flow cytometry-based
399 abundances and pigment-based taxonomic group composition, using relative values, thus normalized against total
400 Chl *a* for pigment-based community composition, and total phytoplankton abundance for both pigment-based and
401 flow cytometry-based phytoplankton groups. For the indicator species analysis, p-values are reported. A Scheirer-

402 Ray-Hare test (non-parametric ANOVA-like test) was performed to determine the significance of Fe-addition and
403 temperature increase, as well as potential interaction effects, on the respective response variable measured. The
404 test was performed for data of the last day of the incubation, since effects were usually strongest then, and some
405 variables were only sampled at the beginning and the end of the experiment (day 6 for A1 and A2, day 8 for W1
406 and W2). We manually calculated eta-squared (η^2 , amount of variance explained, the higher the value, the larger
407 the effect) by dividing the sum of squares of the effect of interest (i.e. iron addition, temperature increase and the
408 interaction between these two) by the total sum of squares. The η^2 is provided when temperature increase, iron
409 addition, and/or the interaction between both tested as significant. Since we wanted to look at the overall effect of
410 Fe addition, temperature increase, and potential interaction effects on total phytoplankton abundances based on
411 flow cytometry, we additionally performed a generalized linear model (GLM), assuming a quasi-poisson
412 distribution in combination with a log-link, including the bioassay as well as the day number as factors without
413 interaction, and including an interaction term for the Fe- and temperature-treatment. For the GLM, the data of all
414 bioassays and all timepoints (excluding day 0) were combined. The formula for the GLM was: total phytoplankton
415 abundances ~ Fe treatment * temperature treatment + bioassay name + day number. Statistical results are only
416 reported for variables where more than 1 replicate was available. We also performed an NMDS analysis based on
417 phytoplankton abundances using the vegan library with Bray-Curtis dissimilarity (seed set to 123). A significance
418 level of $p < 0.05$ was used. Where applicable, the mean \pm standard deviation is reported, unless stated otherwise.
419 All statistical results are reported in the Supplements (Tables S9 – S20).

420

421 **3. Results**

422 **3.1 Sample site characteristics**

423 The *in-situ* temperature was below zero for all bioassays, with lowest values for Amundsen Sea bioassay A2 and
424 Weddell Sea bioassay W2 (-1.6 °C and -1.4 °C, respectively, compared to -0.6 °C and -0.3 °C for A1 and W1).
425 The daily average irradiance at sampling depth on day of sampling was lowest for A1 and A2, i.e., $< 6 \mu\text{mol}$
426 $\text{quanta m}^{-2} \text{s}^{-1}$, compared to 18 and 98 $\mu\text{mol quanta m}^{-2} \text{s}^{-1}$ for W1 and W2. Dissolved inorganic macronutrient
427 concentrations were relatively comparable between bioassays, except the silicate concentration in W1 being ~ 20
428 μM lower than for the other bioassays (but still far from limiting). Initial dFe concentrations in the Weddell Sea
429 were lower compared to the Amundsen Sea (Table 1), as were dMn concentrations (Fig. 2). Bioassay A1 had the
430 highest Chl *a* concentrations (sampled within the ASP), followed by W1. Both bioassays also had the highest
431 share of $>20 \mu\text{m}$ Chl *a*. The Chl *a* concentration of A2 was almost exclusively made up of $< 20 \mu\text{m}$ sized

432 phytoplankton (98% of total Chl *a*, Table 1). Flow cytometry derived phytoplankton abundances were highest for
 433 the Amundsen bioassays. The photosynthetic efficiency F_v/F_m at the start of the incubations was 2-fold lower for
 434 the Weddell Sea bioassays compared to the Amundsen Sea bioassays (i.e., 0.3 vs 0.6 r.u., respectively). The station
 435 for bioassay W2 was closest to the coast, followed by A1, A2 and W1, however distance to land did not seem to
 436 have a major impact on either phytoplankton community composition, or nutrient concentrations.

437

438 **Table 1:** Characteristics of the seawater used for the bioassay experiments. Lat. = latitude, Long. = longitude, Temp =
 439 temperature, Si = silicate, PO₄ = phosphate, NO_x = nitrate + nitrite, dFe = dissolved iron, Chl *a* = chlorophyll *a*, Phyto = total
 440 flow cytometry based phytoplankton abundances, F_v/F_m = photosynthetic capacity of the total phytoplankton. The reported
 441 irradiance is the average irradiance at the sampling depth on the day of sampling.

Bioassay	Station	Lat. (°S)	Long. (°W)	Temp. (°C)	Salinity (psu)	Irradiance ($\mu\text{mol quanta m}^{-2} \text{sec}^{-1}$)	Si (μM)
A1	31	73.50	116.50	-0.6	33.99	5.0	77.9
A2	52	72.00	118.42	-1.6	33.89	3.1	77.5
W1	17	65.00	000.00	-0.3	33.90	17.7	58.3
W2	36	70.08	011.08	-1.4	33.82	97.6	71.8

Bioassay	PO ₄ (μM)	NO _x (μM)	dFe (nM)	total Chl <i>a</i> ($\mu\text{g L}^{-1}$)	< 20 μm Chl <i>a</i> (%)	Phyto ($\times 10^3 \text{mL}^{-1}$)	F_v/F_m r.u.
A1	1.8	24.3	0.28	3.0	42	8.4	0.6
A2	2.0	28.2	0.10	0.4	98	7.1	0.6
W1	1.6	24.0	0.05	1.5	24	5.6	0.3
W2	1.9	27.9	0.03	0.6	65	4.4	0.3

442

443

444 3.2 Nutrient dynamics

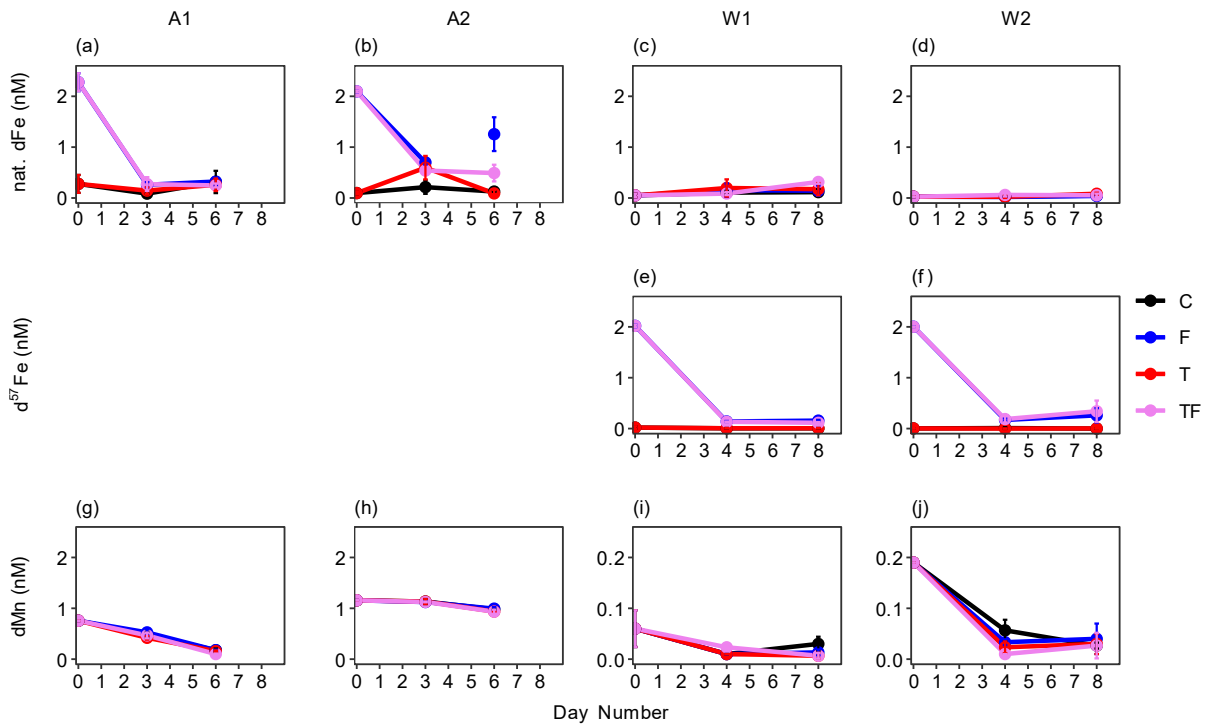
445 Bioassay treatments without Fe addition (C and T) started at naturally low dFe concentrations (0.28 ± 0.16 , 0.10
 446 ± 0.02 , 0.05 ± 0.03 and 0.03 ± 0.01 nM natural dFe for bioassay A1, A2, W1 and W2, respectively), and stayed
 447 within these ranges. The Fe addition treatments (F and TF) showed a rapid (and overall comparable) drawdown
 448 of the added Fe (natural Fe for A1 and A2; Fig 2a, b and $d^{57}\text{Fe}$ for W1 and W2; Fig. 2e, f) in all bioassays,
 449 regardless of its isotopic composition. The dFe concentrations in F and TF treatments (0.29 ± 0.07 nM) at the end
 450 of the bioassays were comparable to concentrations in non-Fe addition treatments (0.28 ± 0.14 nM, Table S8) for

451 the relatively high-Chl *a* bioassay A1. In contrast, bioassay A2 had most dFe left at the end of the incubation (0.80
452 ± 0.46 nM for F and TF, compared to 0.11 ± 0.04 nM for C and T) which concurs with the low starting Chl *a*
453 concentration and irradiance intensity. However, since the average dFe concentration in Fe amended treatments
454 was lower (0.65 ± 0.10 nM) in the middle of the incubation period (day 3, see Figure 2 b), we cannot rule out
455 potential contamination during sampling as a reason for the higher dFe concentrations, notably in the F treatment.
456 For the Weddell Sea bioassays, $d^{57}\text{Fe}$ in F and TF treatments declined rapidly with low final concentrations (0.14
457 ± 0.03 and 0.31 ± 0.17 nM for W1 and W2, respectively) compared to the non-Fe addition treatments (0.01 ± 0.01
458 nM $d^{57}\text{Fe}$ and below detection limit for W1 and W2, respectively). Other trace metals were also measured, and
459 dissolved manganese (dMn) drawdown did not differ between treatments (Fig. 2g-j). However, the starting
460 concentrations of dMn were low for W1 and W2 (0.06 ± 0.03 and 0.19 , SD < 0.01 nM, compared to 0.76 , SD $<$
461 0.01 1.16 ± 0.01 nM for A1 and A2, respectively).

462 The dissolved inorganic macronutrients were not limiting phytoplankton growth during the bioassays. Final
463 concentrations were at least 7.2, 0.3 and 37 μM in all bioassays for nitrogen, phosphate, and silicate, respectively
464 (Supplement Fig. S4). Still, there was discernible drawdown of macronutrients by the microbial community during
465 the incubations, except for Amundsen Sea bioassay A2 (Supplement tables S10, S21). Fe addition (both F and TF
466 treatments) had a significant impact on phosphorous drawdown for bioassays A1, W1 and W2 ($p < 0.05$, η^2 : 0.53,
467 0.76 and 0.76 for A1, W1 and W2, respectively; and on average 0.45 μM lower for Fe addition treatments
468 compared to C) and on nitrogen drawdown for bioassays W1 and W2 ($p < 0.004$, $\eta^2 > 0.75$, average of 9.8 μM
469 lower for Fe addition treatments compared to C). The TF treatment showed stronger drawdowns especially for
470 Weddell Sea bioassays W1 and W2 (average 0.7-fold change between TF and F treatments for both phosphorus
471 and nitrogen, respectively), however there was no significant interaction effect between temperature increase and
472 Fe addition. In contrast, silicate acid concentrations at the end of the incubation period were impacted by the
473 increase in temperature for bioassays A1, A2 and W2 ($p < 0.02$, η^2 : 0.76 for A1 and W2 and η^2 : 0.52 for A2 and
474 $p = 0.06$ and η^2 : 0.32 for bioassay W1), with T treatments showing on average a 2.4 μM lower silicate
475 concentration compared to the control. Only bioassay W1 showed an effect of Fe-addition on silicate drawdown
476 ($p = 0.02$, η^2 : 0.52), resulting in the TF treatment showing lowest concentrations on the last day of the incubations
477 (0.8-fold change compared to the control and 0.9-fold change compared to both T and F treatment). The ratios of
478 silicate drawdown to nitrogen and to phosphorus were higher in W1 than in W2 (i.e., 1.4 and 18.3 in W1 and 0.7
479 and 10.5 in W2). Moreover, when dFe was added, the silicate to nitrogen ratio (Si:N), as well as silicate to

480 phosphorous ratio (Si:P) drawdown was lower in bioassays A1, W1 and W2 compared to non-Fe treatments (0.86
 481 and 1.02 Si:N for Fe and non-Fe treatments and 11.3 and 12.5 Si:P, respectively, Table S10).

482



483

484 **Figure 2:** Average concentrations of natural dissolved Fe (a, b, c, d), $d^{57}\text{Fe}$ (e, f) and $d\text{Mn}$ (g, h, i, j) concentrations for
 485 Amundsen Sea (A1: a, g; A2: b, h) and Weddell Sea (W1: c, e, i; W2: d, f, j) bioassays. Amundsen Sea bioassays did not
 486 receive ^{57}Fe supplementation. The black line represents the control (C) treatment, the red line the temperature (T) treatment,
 487 the blue line the iron (F) treatment, and the purple line the combined temperature and iron treatment (TF). Error bars
 488 indicates the standard deviation ($n = 2$ or 3 , except for $d\text{Fe}$ of bioassay A2 TF treatment day 3), when they are not visible it is
 489 smaller than the symbol. Bioassay A2 showed a higher $d\text{Fe}$ concentration on day 6 compared to day 3, which we cannot
 490 exclude to be due to potential contamination and was thus treated as an outlier.

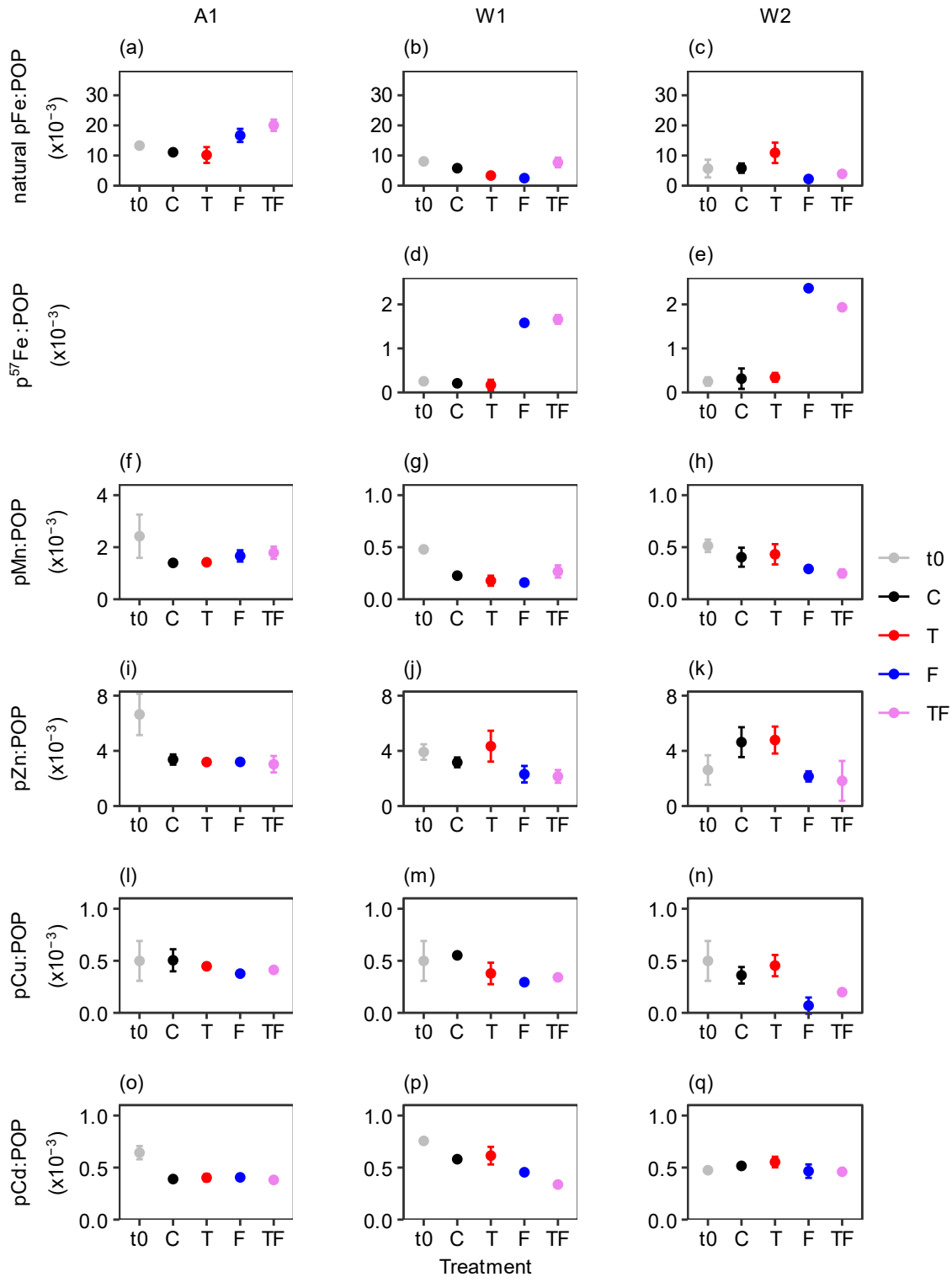
491

492 Particulate Fe concentrations (natural pFe for A1, $p^{57}\text{Fe}$ for W1 and W2) increased over time for the Fe addition
 493 treatments (Table S21 (Metadata), Table S8) in all bioassays examined (excluding A2 as particulate metals were
 494 not measured there), and pFe concentrations at the last day of incubations were (positively) impacted by Fe-
 495 addition ($p \leq 0.01$, $\eta^2 \geq 0.73$ for A1, W1 and W2, final concentrations were 8.01 ± 0.83 , 1.09 ± 0.10 , 0.89 ± 0.33
 496 nM for Fe addition treatments and 4.40 ± 0.21 , 0.08 ± 0.02 , 0.09 , $\text{SD} < 0.01$ nM for treatments without Fe addition
 497 for A1, W1 and W2, respectively).

498 To examine potential differences in phytoplankton trace metal stoichiometry in response to Fe addition and/or
 499 warming, we calculated the ratio of pFe and other trace metals (pMn, pZn, pCd and pCu) to POP concentrations
 500 (Fig. 3, Table S21). The initial lithogenic fraction of particulate trace metals was on average 60% in Amundsen
 501 Sea compared to 52% in the Weddell Sea. Particulate Al, and hence the estimated lithogenic particle
 502 concentrations, remained in the same range between the start and end of the experiments (Table S20) and thus the

503 lithogenic particles provided a consistent background that did not affect observed changes between treatments.
504 Fe-addition significantly increased pFe:POP ratios (natural pFe for A1 and p⁵⁷Fe for W1, W2, Table S11) for all
505 bioassays ($p \leq 0.01$, $\eta^2 \geq 0.73$; average 2.5-fold change for natural pFe:POP (A1) and 13.3-fold change for
506 p⁵⁷Fe:POP in Weddell Sea bioassays for Fe-addition treatments compared to the control). Furthermore, the
507 pMn:POP ratios increased (by 0.33 compared to C) due to Fe-addition in bioassay A1 and decreased (by 0.13
508 compared to C) in W2 ($p < 0.01$ and 0.004, η^2 : 0.74 and 0.76, respectively). For bioassay W1, neither Fe nor
509 temperature alone had a significant impact on the pMn:POP ratio, however, the combination of both treatments
510 tested significant ($p = 0.01$, η^2 : 0.63), with the TF treatment showing an average 1.4-fold changed ratio compared
511 to all other treatments. Also, the pCd:POP ratio was significantly affected by Fe-addition in W1 and W2 ($p < 0.05$,
512 η^2 : 0.76 and 0.39 for W1 and W2), showing decreased values (by on average 0.12) for Fe-addition treatments
513 compared to the control (Fig. 3 o-q), however no effect was seen for bioassay A1. A similar outcome was observed
514 for pZn:POP ratios ($p \leq 0.01$, η^2 : 0.65 and 0.76 for W1 and W2, respectively, by on average 1.8 compared to C).
515 For pCu:POP ratios, a decrease due to Fe-addition was mainly observed in bioassay A1 and W2 ($p < 0.009$, $\eta^2 \geq$
516 0.73, by on average 0.16 compared to C), while for bioassay W1, Fe-addition caused a notable, but not statistically
517 significant effect ($p = 0.09$, η^2 : 0.32, Fig. 3, by on average 0.23 compared to C).

518



519

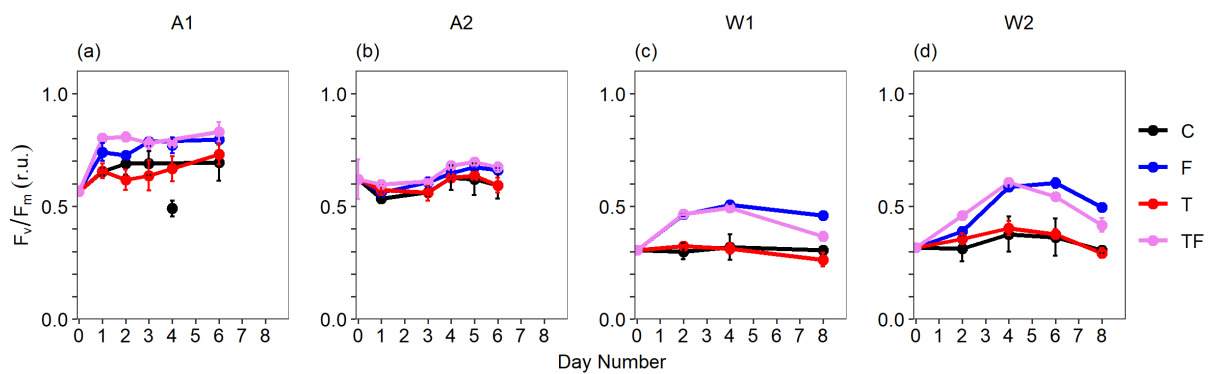
520 **Figure 3:** Average ratios (x10⁻³, mM:M) of particulate trace metal to particulate organic phosphorus (POP) for Amundsen
 521 Sea A1 (a, f, i, l, o) and Weddell Sea W1 (b, d, g, j, m, p) and W2 (c, e, h, k, n, q) bioassays. There is no data available for
 522 A2. pFe = natural particulate, p⁵⁷Fe = particulate iron in the ⁵⁷Fe form (not added to Bioassay A1), pMn = particulate
 523 Manganese, pZn = particulate Zinc, pCu = particulate copper, pCd = particulate cadmium. t0 are starting ratios, whilst ratios
 524 for C (control), T (temperature), F (iron) and TF (combination of temperature and iron) were measured on the last day of the
 525 incubations (day 6 and 8 for Amundsen and Weddell Sea bioassays, respectively). Error bars indicates the standard deviation
 526 (n = 2 or 3), except for bioassay A1, T-treatment for all ratios and bioassay W1 C treatment for the pFe:POP ratio, there n =
 527 1. If the error bar is not visible, then it is smaller than the symbol. Please note the different y-axis ranges for manganese to
 528 POP ratios (f–h).

529 3.3 Photosynthetic efficiency

530 Fe addition led to an increase of F_v/F_m for all bioassays (Fig. 4, $p \leq 0.009$; $\eta^2 > 0.68$ for all bioassays, Table S12),
531 with stronger increases in Weddell Sea compared to Amundsen Sea bioassays (average of 1.42- and 1.14-fold
532 change for Fe addition (F and TF) versus control treatments for Weddell and Amundsen Sea bioassays,
533 respectively). Towards the end of the incubations of W1 and W2, F_v/F_m decreased slightly again for the Fe addition
534 treatments (most so for TF, with final F_v/F_m values being still higher than for C and T treatments), coinciding with
535 Fe depletion (Fig. 2).

536

537



538

539 **Figure 4:** Temporal dynamics of the photosynthetic efficiency (F_v/F_m , relative units) of the phytoplankton for the Amundsen
540 Sea A1 (a), A2 (b) and the Weddell Sea W1 (c) and W2 (d) bioassays. The black line represents the control (C) treatment, the red line the temperature (T) treatment, the blue line the iron (F) treatment, and the purple line the combined temperature and
541 iron (TF) treatment. Averages of triplicates with error bars representing the standard deviation; if not visible it is smaller
542 than the symbol. The control treatment of bioassay A1 showed an outlier for F_v/F_m values on day 4, which was excluded.
543

544

545 3.4 POC, Chl *a*, and phytoplankton taxonomic community composition

546 Total Chl *a* concentration at the start of the incubations (Table 1) was highest for the ASP bioassay A1 ($3 \mu\text{g L}^{-1}$)
547 and lowest for bioassay A2 outside the ASP ($0.4 \mu\text{g L}^{-1}$). Of the Weddell Sea bioassays, W1 had the highest Chl
548 *a* starting concentration (1.5 compared to $0.6 \mu\text{g L}^{-1}$ for W1 and W2). Starting concentrations of total POC in A1
549 and W1 were higher than A2 and W2 (384 and $347 \mu\text{g L}^{-1}$ compared to 91 and $136 \mu\text{g L}^{-1}$, respectively). The POC
550 to Chl *a* ratio was lower for A1 (130) than the other bioassays (212-239). Total POC concentrations did not display
551 differences between treatments at the end of the incubations for A1 and A2 (Fig. 5a-d), yet total Chl *a*
552 concentrations exhibited treatment-specific differences for all bioassays (Fig. 5e-h, Table S13). Only bioassays
553 W1 and W2 showed a significant increase in bacterial abundances with Fe addition (final abundance 4.7 ± 0.9 ,
554 4.5 ± 0.5 vs 3.1 ± 1.0 and 4.7 ± 0.6 , 5.4 ± 0.2 vs 4.4 ± 0.1 for F, TF vs C treatments in W1 and W2, respectively,
555 Table S12). However, bacteria did not have a major effect (less than 3%) on total POC concentrations. Fe-addition

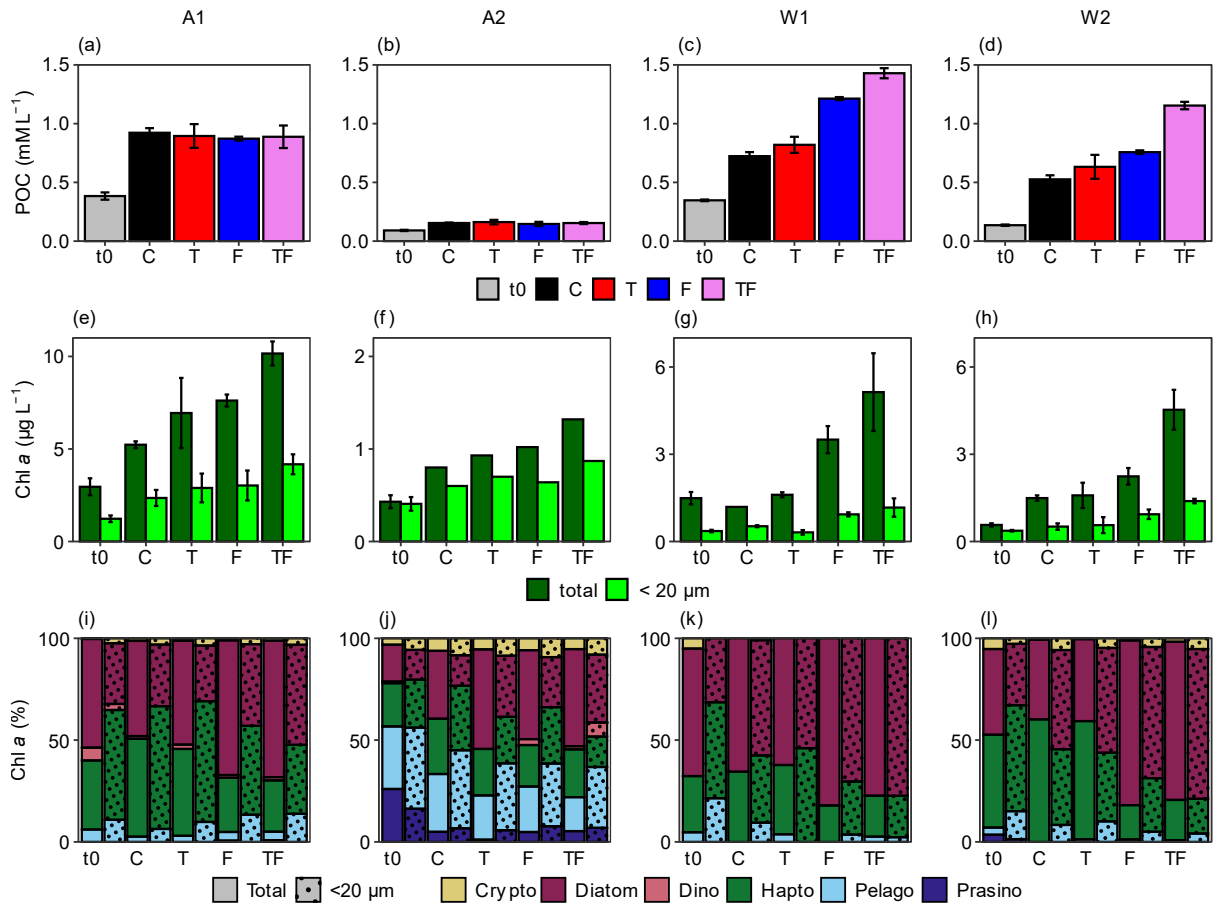
556 always positively impacted Chl *a* concentrations (p : 0.02, 0.005 and 0.006, η^2 : 0.52, 0.76 and 0.67 for bioassays
557 A1, W1 and W2; not tested for A2 due to $n = 1$ for all Chl *a* samples and W1 C due to $n = 1$), however the effect
558 was stronger in Weddell Sea Bioassays (average of 1.6- and 2.9-fold difference for Amundsen and Weddell Sea
559 with Fe addition compared to C). Amundsen Sea bioassays also showed a slight increase in Chl *a* with increased
560 temperatures. Strongest treatment-specific increases in Chl *a* concentrations were, however, obtained for the TF
561 treatment in all bioassays, resulting in an average of 1.7 μg more Chl *a* L^{-1} compared to the F treatment. POC
562 concentrations in W1 and W2 showed similar treatment responses as total Chl *a* in these bioassays.

563 The TF treatment also caused the strongest increase for the $< 20 \mu\text{m}$ Chl *a* fraction (Fig. 5 e–h) for all bioassays,
564 and Fe-addition generally had a positive impact on $< 20 \mu\text{m}$ Chl *a* concentrations, with effects being strongest in
565 both Weddell Sea bioassay W1 and W2 (increases of 1.2, 0.2, 0.5 and 0.7 μg L^{-1} for A1, A2, W1 and W2 compared
566 to the control, respectively and $p = 0.04$ and 0.006, η^2 : 0.37 and 0.67. A2 and W1 were not tested due to missing
567 replicates). The $< 20 \mu\text{m}$ fraction at the start of the bioassays made up respectively 42, 24 and 65 % of total Chl *a*
568 in A1, W1 and W2, whereas for bioassay A2 95 % of the total Chl *a* concentration was $< 20 \mu\text{m}$. At the end of
569 the bioassays, shares were 42, 25, 35 % and 70 % for A1, W1, W2 and A2, respectively.

570 Diatoms dominated the phytoplankton community at the start of A1 and W1 (53 and 62 % of total Chl *a*), followed
571 by haptophytes (34 and 27 %; Fig. 5i-l). Bioassay W2 had a comparable share of diatoms and haptophytes (42
572 and 46 % of total Chl *a*), whilst the phytoplankton community of A2 was taxonomically most diverse.

573 Diatoms showed in general a strong response to Fe addition (F and TF treatment) and could be defined as an
574 indicator group for Fe addition treatments in A1 and W2 ($p < 0.005$). Absolute diatom abundances increased as
575 well with Fe-addition, especially for the TF treatment, in bioassays A1 (F and TF treatment, $p = 0.007$) and W2
576 (TF treatment, $p = 0.02$, Table S21). In bioassay W2, diatoms also showed a higher share for Fe addition treatments
577 in the $< 20 \mu\text{m}$ fraction ($p < 0.05$), with absolute abundances being higher in the TF treatment for bioassays A1,
578 W1 and W2 ($p < 0.04$), and bioassay W1 also showing higher abundances at the F treatment ($p = 0.04$). The
579 contribution of haptophytes declined (in response to the diatom increase, also in W1 where the diatom response
580 was not significant, $p < 0.007$), however their absolute concentration (in μg Chl *a* L^{-1} ; Table S21) did not decline
581 except for the F-treatment in bioassay W2 ($p = 0.01$). Both the share ($p = 0.01$) and absolute concentration ($p =$
582 0.04) of pelagophytes increased with Fe addition in the $< 20 \mu\text{m}$ fraction of bioassay A1. Cryptophyte abundances
583 increased in the total fraction of the TF treatment for A1 and W2 ($p = 0.02$ and 0.01, respectively), and the < 20
584 μm fraction in W1 ($p = 0.02$), however their share did not change with treatments.

585



586

587 **Figure 5:** Average concentrations of particulate organic carbon (POC, a-d), total and < 20 μm (dotted columns) Chl *a* (e-h),
 588 and the taxonomic composition of the phytoplankton community (i-l, % of total Chl *a*) for the Amundsen Sea A1 (a, e, i)
 589 and A2 (b, f, j), and the Weddell Sea W1 (c, g, k) and W2 (d, h, l) bioassays. Error bars represent the standard deviation (n =
 590 3 except when no error bar is shown, then n = 1). t0 = starting conditions, C = control, T = temperature treatment, F = iron
 591 addition treatment, TF = temperature and iron addition treatment. For i-l, Crypto, Dino, Hapto, Pelago and Chloro stands for
 592 cryptophytes, dinophytes, haptophytes, pelagophytes and chlorophytes, respectively. Solid bars represent the total and
 593 shaded bars the < 20 μm fraction community composition. Note the difference in y-axis for the Chl *a* panels e-h.

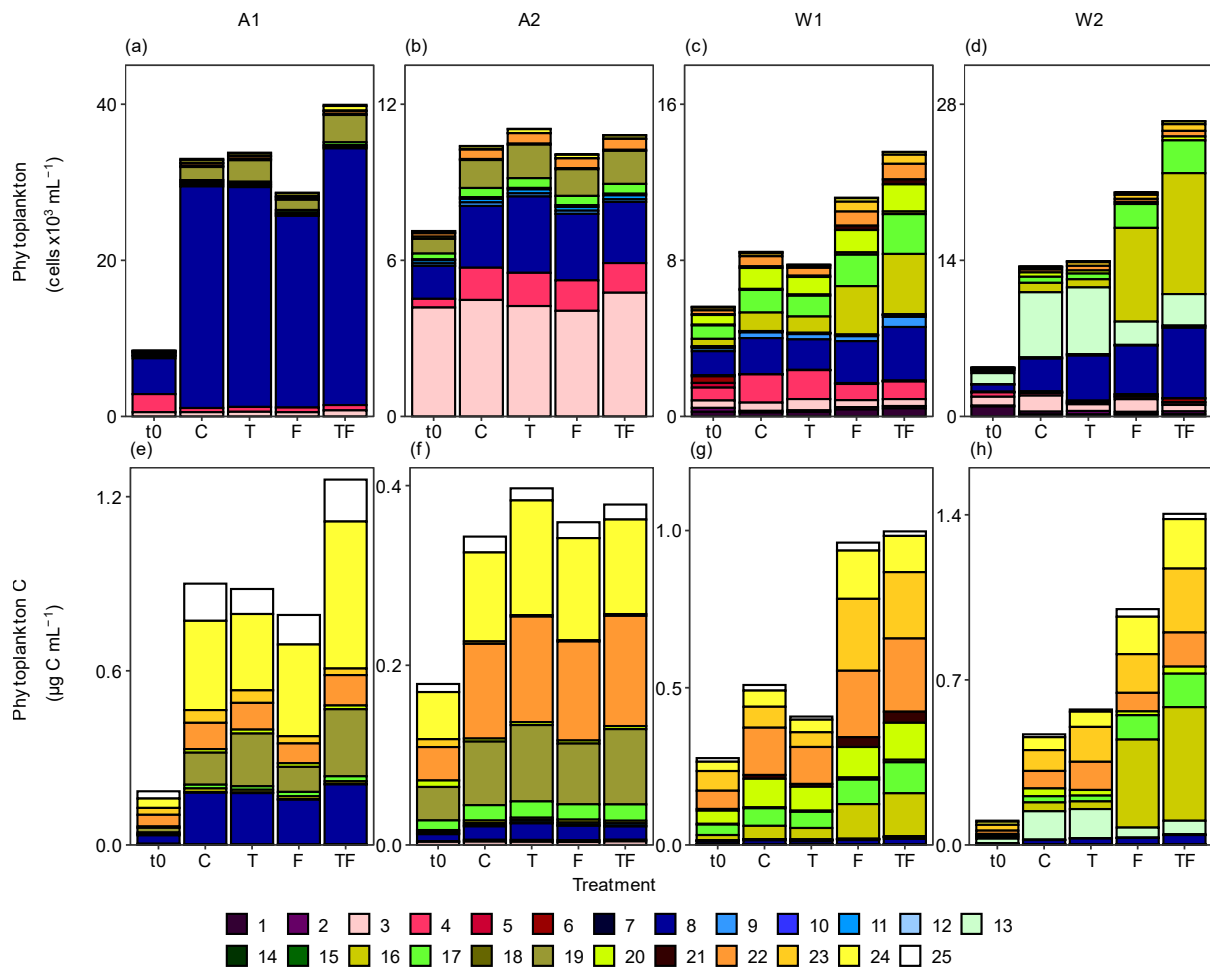
594

595 3.5 Phytoplankton abundances

596 The total abundances of < 20 μm phytoplankton (Fig. 6, Fig. S5, Table S21) increased with time for all bioassays
 597 and the treatment-specific dynamics largely mimicked the responses observed for the < 20 μm Chl *a* fraction (Fig.
 598 5e-h, Table S12). Bioassay A1 had overall the highest phytoplankton abundances (up to $40,000 \pm 4,000$ cells mL⁻¹
 599 ¹ for the TF treatment; Fig. 6a) and was dominated by *Phaeocystis antarctica* Phyto 8 (highest abundances of
 600 $37,053$ mL⁻¹ were observed in the TF treatment; Table S21). Phyto 19 increased in abundance and share (Fig. 6a,
 601 Table S14) specifically in the temperature treatments, with net growth rates of 0.40 ± 0.08 d⁻¹ and 0.52 ± 0.005 d⁻¹
 602 ¹ for the T and TF treatments (compared to 0.35 ± 0.11 d⁻¹ and 0.30 ± 0.09 d⁻¹ for C and F treatments, $p < 0.04$,
 603 Table S15) and final abundances of $2,800$ and $3,500$ cells mL⁻¹ for T and TF (compared to $1,700$ and $1,300$ mL⁻¹
 604 for C and F, $p < 0.01$). Phyto 3 also showed higher abundance-derived net growth rates with warming (0.33 ± 0.13
 605 and 0.32 ± 0.002 vs 0.26 ± 0.06 d⁻¹ for the T, TF and C treatment, respectively), but with abundances being only

606 significantly higher for the TF treatment (776 ± 37 vs 542 ± 107 cells mL^{-1} for TF and C treatments). Phyto 24
 607 was positively impacted by Fe addition, particularly the TF treatment resulted in higher net growth rates and final
 608 abundances (i.e., 0.32 ± 0.09 vs 0.15 ± 0.06 d^{-1} , and 595 ± 62 vs 361 ± 9 cells mL^{-1} for TF compared to the C
 609 treatment; $p < 0.05$). When converted to cellular carbon based on cell volume using 237 and 196.5 $\text{fg C } \mu\text{m}^{-3}$ as
 610 conversion factors for Pico- and Nanophytoplankton, respectively (Fig. 6e), the strong positive response of the
 611 phytoplankton to the TF treatment was mostly due to this larger-sized Phyto 24 (average diameter of 19 μm , $p =$
 612 0.01, stat: 0.92) and to smaller extent Phyto 19 ($p < 0.01$).

613



614

615 **Figure 6:** Flow cytometry-based phytoplankton community composition (a-d) and carbon (e-h) at the start (t0) and the end
 616 of the bioassay incubations for the different treatments (average of triplicates) for Amundsen Sea bioassays A1 (a, e), A2 (b,
 617 f), and Weddell Sea bioassays W1 (c, g) and W2 (d, h). t0 = starting conditions, C = control, T = temperature treatment, F =
 618 iron addition treatment, TF = temperature and iron addition treatment. Phytoplankton groups are sorted by size, with Phyto 1
 619 – 6 $\leq 3 \mu\text{m}$, Phyto 7 – 20 $\leq 10 \mu\text{m}$ and Phyto 21 – 25 $\geq 10 \mu\text{m}$. Phyto 5, 6, 7, 11, 12 and 14 are cryptophytes, Phyto 20, 22 –
 620 25 diatoms and Phyto 8 *Phaeocystis antarctica*. Note the different scales.

621

622 Bioassay A2 presented the highest share of picoeukaryotes, especially Phyto 3 (59 % compared to max. 18 % in
 623 the other bioassays, Fig. 6b). Only few treatment-specific responses were recorded. Phyto 19 increased somewhat

624 with warming ($p = 0.04$), and Phyto groups 16 and 17 showed increased net growth rates with Fe addition (0.31
625 ± 0.22 and 0.23 ± 0.06 vs 0.09 ± 0.16 and 0.31 ± 0.06 , 0.30 ± 0.06 and 0.23 ± 0.06 for the F, TF and C treatments
626 of Phyto 16 and 17, respectively, $p < 0.02$ for both, Table S14, Table S16). The phytoplankton populations in W1
627 were distributed more equally (Fig. 6c), with higher abundances of especially Phyto 16 and 17 for the Fe addition
628 treatments ($p < 0.05$, most pronounced for TF with average abundances of $3,103 \pm 1,290$ vs 948 ± 218 cells mL^{-1}
629 and $2,041 \pm 572$ vs $1,158 \pm 216$ cells mL^{-1} for Phyto 16 and 17 in the TF vs C treatments, respectively, Table S14).
630 Their specific net growth rates were up to 2.2-fold higher for the Fe addition treatments than the control ($0.29 \pm$
631 0.02 , 0.38 ± 0.10 and 0.20 ± 0.02 , and 0.16 ± 0.02 , 0.21 ± 0.06 and 0.09 ± 0.02 d^{-1} for the F, TF and C treatment
632 of Phyto 16 and 17, Table S17). When expressed in carbon, Phyto 16 was still a recognisable indicator species (p
633 $= 0.03$) but at the same time the larger-sized Phyto 21 (average cell diameter of 10 μm) and diatoms Phyto 22-24
634 (13-19 μm) showed clear positive responses to Fe addition (Fig. 6g, $p < 0.05$ for all). Net growth rates were largely
635 comparable for these phytoplankton groups: 0.23 ± 0.02 , 0.19 ± 0.01 , 0.17 ± 0.04 , 0.20 ± 0.05 d^{-1} for Phyto 21-24
636 in the F treatment (and similar net growth rates in the TF treatment) compared to 0.09 ± 0.07 , 0.14 ± 0.03 , $0.04 \pm$
637 0.04 , 0.12 ± 0.02 in the C treatment, respectively ($p < 0.03$). Bioassay W2 also showed a distinct shift in favour
638 of Phyto 16 and Phyto 17 (away from Phyto 13) with Fe addition, already early in time (Table S21), both for
639 abundances and cellular carbon (Fig. 6d, h, $p < 0.01$ for all, Table S14). The F treatment net growth rates of Phyto
640 16, 17 and Phyto 13 were 0.42 ± 0.02 , 0.34 ± 0.03 and 0.21 ± 0.09 d^{-1} (again with similar growth in the TF
641 treatments) compared to 0.20 ± 0.03 , 0.17 ± 0.04 and 0.37 ± 0.02 d^{-1} in the C treatment ($p < 0.03$, Table S18).
642 Diatoms 23 and 24 also responded positively to Fe addition with ~ 2 -fold higher net growth rates than the control
643 (Fig. 6h, $p < 0.01$). Phyto 23 net growth rates were 0.37 ± 0.06 and 0.39 ± 0.04 d^{-1} for F and TF compared to 0.19
644 ± 0.06 d^{-1} for the C treatment ($p = 0.004$), and Phyto 24 net growth rates were 0.38 ± 0.08 and 0.32 ± 0.05 for F
645 and TF treatments vs 0.22 ± 0.09 for the C treatment. Phyto 19 was the only phytoplankton population that
646 showed a consistent selective positive response (in share) to warming (and not to Fe addition) in the Amundsen
647 Sea bioassays. Diatom Phyto 22 increased with temperature in bioassay W2 ($p \leq 0.01$). We refer to Table S21 for
648 less pronounced responses of the other phytoplankton populations. Overall, the response by the larger
649 phytoplankton populations is also illustrated by the higher average cellular biovolumes in the F and TF treatments
650 of W1 and W2 (Fig. S6). The Amundsen Sea bioassays did not show a treatment-specific increase in
651 phytoplankton biovolume. Fe-addition had a significant effect on total phytoplankton abundances for Weddell
652 Sea bioassays ($p < 0.02$, η^2 : 0.56 and 0.74 for W1 and W2, with Fe addition leading to an average 1.6-fold change
653 compared to C). The GLM we performed (explained deviance: 86 %), indicates an interaction effect of Fe-addition

654 and warming ($p = 0.03$ for the interaction, exponentiated coefficient (ec): 1.13), i.e. Fe-addition of 2 nM in
655 combination with a 2 °C temperature increase led to an overall increase in algal abundances of about 28 %. Fe-
656 addition (ec: 1.03), temperature increase (ec: 1.11), bioassay and day number ($p < 0.001$ for all, for other statistical
657 parameters, see Table S20) were also significant explanatory factors. The NMDS analysis of the Weddell Sea
658 bioassays (Fig. S7c, d) demonstrated clear distinction between the Fe addition treatments and the non-addition
659 treatments after the second day of the incubations. For bioassay W1, the TF and T treatments clustered on the last
660 day of incubation separately from the F and C treatments, respectively. For bioassay W2, the T treatment also
661 separated on the last day while the TF and F treatments remained closer together. Bioassays A1 and A2 did not
662 display obvious clustering by treatment, other than time (i.e., separation after day 2).

663

664 **4. Discussion**

665 **4.1 Trace metal and macronutrient dynamics**

666 The pFe concentrations showed the expected significant increase in the Fe addition treatments for both Amundsen
667 (natural dFe added) and the Weddell Sea bioassays (d⁵⁷Fe added) at both temperatures, indicating that the added
668 dFe was indeed taken up and incorporated in the phytoplankton cells. Additionally, in bioassay W2 the final p⁵⁷Fe
669 in the TF treatment was higher than in the F treatment (1.12 ± 0.11 nM compared to 0.66 ± 0.20 nM),
670 demonstrating enhanced Fe uptake with higher temperatures.

671 The higher starting concentrations of dFe in the Amundsen Sea, compared to the Weddell Sea, can be attributed
672 to the Fe input from basal melt (Rignot et al., 2013). Conversely, the naturally low dFe concentrations in the
673 Weddell Sea underscore the area's limited Fe input (e.g., de Baar et al., 1990; Klunder et al., 2011). Fe is needed
674 in nitrate assimilation and as such uptake of nitrate is coupled to the Fe nutritional status (Schoffman et al., 2016,
675 Milligan and Harrison, 2000). Similarly, diatom cellular silicate to nitrogen ratios are known to increase in
676 response to Fe stress (Meyerink et al., 2017). Highest drawdown of the macronutrients typically occurred in the
677 TF treatment, which also showed the largest phytoplankton accumulation (Table S20, Table S21). However,
678 whilst dissolved inorganic phosphate and nitrogen drawdown was mostly affected by Fe addition, silicate
679 drawdown in bioassays A1 and W2 was more impacted by temperature. Despite a lower Chl *a* concentration (both
680 total and $< 20 \mu\text{m}$) and phytoplankton abundance for the T than the TF treatment in these bioassays, the silicate
681 drawdown was comparable. Although Fe stress is reported to cause reduced cellular Chl *a* concentrations
682 compared to Fe replete conditions (Greene et al., 1992), it is an unlikely cause as the total phytoplankton
683 abundances displayed similar differences between the T and TF treatment compared to $< 20 \mu\text{m}$ Chl *a*

684 concentrations. Instead, higher temperature may have stimulated Si uptake, as reported for the diatom
685 *Pseudonitzschia seriata* at temperatures above 0 °C (Stapleford & Smith, 1996). It might also be that the T
686 treatment experienced higher Fe stress than the control, which is also known to increase Si uptake (Meyerink et
687 al., 2017). However, since phytoplankton abundances, F_v/F_m and Chl *a* concentrations were not higher in T
688 treatments compared to the control, and since phytoplankton requires less Fe at higher temperatures (Jabre &
689 Bertrand, 2020), this is less likely. Bioassay W1 showed the strongest decline in silicate concentrations, with both
690 temperature and Fe affecting silicate drawdown. The relatively high fraction of diatoms (and specifically the large-
691 sized Phyto 20 and 22-24) in bioassay W1 could theoretically have caused the strong silicate drawdown and high
692 ratio of silicate relative to nitrogen (or phosphorus) uptake for all treatments. However, A1 also had high diatom
693 abundances and over the course of the incubations the concentration of diatoms in W2 became comparable to W1.
694 An alternative explanation may be that Mn stress in W1 (0.06 ± 0.04 vs 0.19 ± 0 nM in W1 and W2, respectively)
695 enhanced Si uptake, similar to Fe stress (Hutchins & Bruland, 1998). Increased Si uptake by diatoms under a
696 combined Fe and Mn limitation may possibly enhance protection against grazers (Assmy et al., 2013; Ryderheim
697 et al., 2022) and/or enhance sinking to more nutrient-rich depths (Waite & Nodder, 2001). Considering an
698 increasing awareness of trace metal co-limitation of phytoplankton growth (Wu et al., 2019; Browning et al.,
699 2021; Balaguer et al., 2022; Burns et al., 2023), we recommend further investigation into these potential
700 interactions and their ecological relevance in future studies.

701 Dissolved Mn is known to (co-)limit Southern Ocean phytoplankton growth and community composition together
702 with Fe (Browning et al. 2021, Balaguer et al. 2022). Under such conditions, Fe addition alone positively impacts
703 Chl *a* concentrations, phytoplankton abundances and POC concentrations, but a combination of dFe and dMn
704 addition can lead to higher increases in these variables (Pausch et al. 2019, Browning et al., 2021). Nevertheless,
705 dMn addition effects can often be masked by the effects of Fe addition (Latour et al. 2023), and Fe addition alone
706 can already lead to increases in Chl *a* even in primarily Mn-limited areas (Browning et al., 2021). This fits our
707 results showing increases in Chl *a* concentrations with Fe addition. Also net growth rates based on total
708 phytoplankton abundances showed increases (i.e. 1.5 (0.20 ± 0.05 vs 0.12 ± 0.02 d⁻¹) and 1.4-fold (0.24 ± 0.01
709 vs 0.18 ± 0.01 d⁻¹) higher for Fe-addition treatments (F and TF) compared to the control for bioassays W1 and
710 W2. The lower starting concentrations of dMn in W1 compared to W2 may have contributed to the 2-fold lower
711 phytoplankton net growth rates in W1 compared to W2, independent of the treatment. Our data indicate potential
712 dMn/dFe colimitation in the Weddell Sea already in early summer. Since the requirements for dMn and dFe differ
713 between different phytoplankton groups (Arrigo, 2005; Twining & Baines, 2013; Balaguer et al., 2023), we

714 suggest that the (co-)limitation of dMn and dFe may be affected by phytoplankton community composition.
715 Considering that Mn limitation can be seasonal (Latour et al., 2023), we also urge to study different stages of the
716 phytoplankton bloom period.

717

718 **4.2 Micronutrient stoichiometry**

719 The observed pFe:POP ratios increased upon the addition of iron (natural pFe for bioassay A1 and p⁵⁷Fe for
720 bioassays W1 and W2), validating the experimental design and confirming the uptake of added dFe by
721 phytoplankton. For other bio-essential (Mn, Zn, Cu) or bio-active (Cd) metals, the metal:POP ratio is expected to
722 be elevated under Fe stress due to upregulation of non-specific divalent metal transporters under Fe stress (e.g.,
723 Kustka et al., 2007; Lane et al., 2008) or the increased uptake of phosphorous relative to metals under Fe replete
724 conditions (growth-dilution; Cullen et al., 2003). Specifically for Mn, this might also be due to a higher cellular
725 Mn requirement under Fe stress (Peers & Price, 2004). The pMn:POP ratios were indeed higher in the C and T
726 treatments compared to the F and TF treatments of W2, but for W1, no consistent effect of Fe was observed (Fig.
727 3). In contrast, slightly elevated pMn:POP ratios were observed after Fe addition in A1 (F and TF treatments),
728 matching findings by McCain et al. (2021) and Hawco et al. (2022), showing increased Mn demand in
729 environments with high Fe concentrations. This duality in the pMn:POP ratios is not surprising as Mn demand
730 may not only increase under Fe stress, but it should also increase with Fe addition, as both Mn and Fe are required
731 for photosynthesis (Raven 1990, McCain 2021, Hawco et al. 2022). Hence, in an environment with low dMn
732 concentrations, Fe addition can consequently lead to Mn limitation (e.g., Hawco et al., 2022). Dissolved Mn
733 concentrations at the start of bioassay A1 were relatively high, and indeed pMn:POP ratios increased with Fe
734 addition, while concentrations of dMn decreased during the experiment. However, the low (potentially
735 phytoplankton growth limiting) dMn concentrations in Weddell Sea bioassays from the start might have prevented
736 a noticeable positive effect of Fe addition on Mn uptake. The higher biomass and cell abundance after Fe addition
737 in these experiments implies the community had to make due with less Mn per cell than in the treatments without
738 Fe addition (likely resulting in relatively low Mn quota despite elevated demand), potentially explaining why
739 there was an increase in the pMn:POP ratios in the C and T treatments of W2, whereas this was not observed in
740 W1 with even lower dMn starting concentrations. Such variation in apparent Mn demand and quotas likely reflects
741 adaptive changes in nutrient uptake and storage mechanisms under nutrient stress but could also be due to different
742 phytoplankton community compositions and/or environmental conditions. For example, Twining et al. (2004)
743 observed elevated pMn:POP ratios in individual diatom cells under iron deplete conditions, relative to iron replete

744 conditions, whereas the trend was opposite for autotrophic flagellated cells. However, diatoms were dominant in
745 the F and TF treatments in all experiments, suggesting that other factors besides differences in community
746 composition play a role. Since dMn levels are thought to increase with Fe input (e.g., due to ice shelf melting;
747 Van Manen et al., 2022), we recommend including dMn in future studies examining the effects of global climate
748 change on phytoplankton growth.

749 Besides Mn, other trace metals are known to have variable ratios with respect to POP under different
750 environmental conditions. For example, cellular Cu requirements increase under Fe limitation (Schoffman et al.,
751 2016), which could explain the higher pCu:POP ratios in the C and T treatment compared to the Fe addition
752 treatments in all bioassays analysed (Fig. 3). Similarly, the pZn:POP ratios were also elevated in the non-Fe
753 treatments in W1 and W2, akin to the pCd:POP ratios especially in W1, suggesting higher uptake of metals under
754 Fe limitation as previously suggested (Cunningham & John, 2017). This trend of increased uptake of essential
755 (manganese, zinc, copper) and non-essential metals (cadmium) under dFe limitation underscores the adaptive
756 strategies employed by phytoplankton in navigating nutrient scarcities, emphasizing the complexity of nutrient
757 interactions and their collective impact on phytoplankton ecology under varying environmental conditions (e.g.,
758 Cunningham and John, 2017). Due to the importance of nutrient uptake in the Southern Ocean for the
759 stoichiometry of global nutrient distributions, notably at lower latitudes (Sarmiento et al., 2004; Middag et al.,
760 2020), changes in (micro-)nutrient consumption in the Southern Ocean can have global ramifications for both
761 productivity and ecosystem structure (Moore et al., 2018) which should be further explored in future (modelling)
762 studies. Future studies underpinning these stoichiometric ratios with molecular measurements (e.g., protein
763 expression patterns) could provide further insight into the processes underlying trace metal uptake and use within
764 phytoplankton.

765

766 **4.3 Impact of F and T treatments on Phytoplankton Dynamics**

767 The Weddell Sea bioassays exhibited stronger Chl *a* accumulation, a stronger increase in F_v/F_m and increased
768 phytoplankton abundances in response to Fe addition than the Amundsen Sea bioassays, which is likely due to
769 the lower dFe concentrations (and hence higher degree of Fe limitation for the phytoplankton typical for the
770 Weddell Sea) at the start of the incubations. Indeed, given that the Weddell Sea bioassays were performed early
771 in the productive season, these results imply more severe Fe limitation in the Weddell Sea whereas any Fe
772 limitation in the Amundsen Sea likely only develops later in the season. Consistent with the lower dFe
773 concentrations was the reduced *in-situ* F_v/F_m of the phytoplankton in W1 and W2, which stayed low for non-Fe

774 addition treatments throughout the experiments, as it is a common indicator of Fe stress in the Southern Ocean
775 (Greene et al., 1992; Mills et al., 2012; Olson et al., 2000; Jabre and Bertrand, 2020). In addition, the low dMn
776 concentration may have contributed to the low F_v/F_m (Wu et al., 2019). The decrease in F_v/F_m in the F and TF
777 treatments towards the end of the Weddell Sea bioassays seem to indicate that the added Fe had depleted again to
778 limiting conditions or that Mn became (co-)limiting.

779 The location the seawater for bioassay W1 was taken has similar coordinates as bioassay S54-65 in a study by
780 Viljoen et al. (2018). These authors sampled 3 weeks later (different year) and at a comparable depth (30 m vs 20
781 m in our study) and found largely similar responses by the phytoplankton to Fe addition, i.e., total Chl *a* increased
782 by $\sim 2 \mu\text{g Chl } a \text{ L}^{-1}$ and diatoms dominated the phytoplankton community. In contrast to W1 but comparable to
783 our other bioassays, total Chl *a* concentration in bioassay S54-65 (Viljoen et al. 2018) increased in the control
784 over the duration of the bioassay. The lack of increase in Chl *a* in the control (and T) treatment of W1 might be
785 explained by a lower in-situ dFe for W1, indicating a stronger limitation of dFe. At the same time, POC (and < 20
786 $\mu\text{m Chl } a$) concentrations did show an increase over time in the control treatment of bioassay W1. Moreover,
787 bioassay W2, with even lower starting concentrations of dFe, showed an increase in Chl *a* over time for the control.
788 Given the lowest dMn concentrations in W1, it might be that dMn and not (only) dFe was limiting the production
789 of reaction centres (Raven et al.; 1990), resulting in Chl *a* concentrations to not increase. Given the increased
790 requirement for Mn under low Fe (Peers & Price; 2004), Fe addition may have relieved Mn limitation in the Fe
791 addition treatments slightly, resulting in the observed increase of Chl *a* in those treatments

792 While for the Weddell Sea bioassays the POC concentrations followed comparable responses to total Chl *a* upon
793 Fe addition (Fig. 5), the POC concentrations in the Amundsen Sea bioassays did not. The relatively low Chl:POC
794 ratios in the Weddell Sea bioassays (average over all treatments 0.003 ± 0.003 vs 0.008 ± 0.002 for the Amundsen
795 Sea bioassays) may indicate stronger Fe limitation, since Fe limited cells are known to have a lower Chl:POC
796 ratio compared to non-limited cells (Moore et al. 2007). Alternatively, acclimation to the lower irradiance during
797 the incubations of A1 and A2 led to the higher Chl *a*:POC ratios at the end of incubations (Laws & Bannister,
798 1980; Geider, 1987; Geider et al., 1998; Wang et al., 2009). Despite the low light intensities in Amundsen Sea
799 bioassays, Chl *a* concentrations and phytoplankton abundances in the control treatment increased over time
800 (especially in A1, net growth rate based on total abundances of $0.25 \pm 0.03 \text{ d}^{-1}$), which indicates that the
801 phytoplankton communities were low light adapted. Low light conditions are common for Amundsen Sea
802 phytoplankton (Schofield et al., 2015; Park et al., 2017) but still, the very low irradiance in A2 seemed to have
803 limited growth ($0.09 \pm 0.01 \text{ d}^{-1}$) as also illustrated by incomplete depletion of the dFe added (after 6 days of

804 incubation). The high initial F_v/F_m values suggest that the phytoplankton may not have been limited by dFe (under
805 these low light conditions) and would only require more dFe once light intensities increased again (Strzepek et
806 al.; 2019, Vives et al.; 2022, Latour et al.; 2024). The small increase in F_v/F_m in the Fe addition treatments may
807 suggest growth became dFe limited during the incubation (Fe-addition did show a significant effect on F_v/F_m at
808 the last day of the incubations), despite the light conditions remaining low. Considering diatoms being the
809 taxonomic group responding strongest to Fe additions (Noiri et al., 2005; Feng et al., 2010; Hinz et al., 2012;
810 Mills et al., 2012; Zhu et al., 2016), the low proportion of diatoms at the start of A2 may also have delayed a
811 measurable effect of Fe addition.

812 Although earlier studies reported positive responses of phytoplankton to Fe addition also under low light
813 conditions (Viljoen et al., 2018; Alderkamp et al., 2019), the light intensities used for the low light treatment in
814 those studies were still relatively high (i.e., 15 and 30 $\mu\text{mol quanta m}^{-2} \text{ s}^{-1}$) and well above those in A1 and A2
815 (average of 3.4 and 1.5 $\mu\text{mol quanta m}^{-2} \text{ s}^{-1}$). In addition to higher light levels, the lower initial dFe concentrations
816 in the Ross Sea study (Alderkamp et al. 2019) compared to our study indicate a stronger Fe limitation and
817 subsequently a stronger response to Fe addition. A recent study on Southern Ocean deep chlorophyll maximum
818 phytoplankton responses to Fe addition (Latour et al., 2024) reported a Chl *a* increase at low light intensities
819 (similar to our Amundsen Sea bioassays) and no change of POC (similar to bioassay A2) until light levels
820 increased. This supports our suggestion that the low light condition in A2 was a determining factor for the lack of
821 a response to Fe addition.

822 Future light conditions in the Southern Ocean will vary for the different regions, e.g., lower sea ice coverage may
823 enhance light availability (Leung et al., 2015; Petrou et al., 2016; Krumhardt et al., 2022), whereas increased cloud
824 coverage in the Antarctic Circumpolar Current region would reduce it (Grise et al., 2013; Kelleher and Grise,
825 2022; Krumhardt et al., 2022). Moreover, there are conflicting reports about whether mixed layer depths will
826 increase (Leung et al., 2015) or decrease (Krumhardt et al., 2022), which directly impacts light conditions for the
827 phytoplankton. Our results from the low light bioassay A2, showing only a small effect of Fe on phytoplankton,
828 suggest that in regions or periods with low light, Fe increase will not drastically stimulate phytoplankton growth.
829 This highlights the importance of including light availability in Southern Ocean ecosystem (modelling)
830 predictions.

831 Temperature alone showed a limited effect on phytoplankton, with only 3 phytoplankton groups (Phyto 3, Phyto
832 19 and diatom Phyto 22) increasing in abundances, and only Phyto 19 showing a consistent effect. Still, these
833 groups represent pico-sized as well as larger phytoplankton (2, 8.1 and 13.3 μm diameter). Earlier studies also

834 showed temperature to have only a limited effect on (natural) phytoplankton communities (Rose et al., 2009).
835 Indirect effects of warming (e.g., locally high ice-melt induced freshening, dFe increase) will likely have larger
836 impact on phytoplankton community compositions. Ice-melt induced freshening already led to a shift from diatom
837 to cryptophyte and flagellate dominated communities in the Western Antarctic Peninsula region (reviewed by
838 Deppeler and Davidson 2017), and increased dFe concentrations will affect phytoplankton community
839 composition even more so when combined with temperature increases (this study; Rose et al. 2009). Furthermore,
840 the availability of dFe is likely changing due changes in sources (see introduction) but is also influenced by
841 siderophore production (reviewed by Gledhill and Buck, 2012) but warming of the Southern Ocean does not seem
842 to have a direct effect (Sinha et al., 2019). Warming likely increases the growth rates of siderophore producing
843 bacteria (Sinha et al. 2019), but this may be countered by reduced siderophore production due to ocean
844 acidification (Sinha et al. 2019). Overall, predictions about future conditions and their consequences are complex
845 and have large uncertainty, but it seems likely conditions will be temporally and spatially heterogenous with
846 varying changes in temperature and availability of Fe (and light). For example, while the warming of surface
847 water in the Amundsen Sea has already been observed, Weddell Sea surface temperatures for the deep basin seem
848 relatively stable at the moment with significant warming only below 700 m (Strass et al., 2020). However,
849 upwelling of this warm water leads to local temperature increases in notably coastal regions (Darelius et al., 2023),
850 potentially increasing future temperatures by over 2 °C warmer in troughs that connect the open ocean to ice shelves
851 (Teske et al., 2024), increasing not only temperatures but likely also glacial melt derived Fe supply. This makes
852 it prudent to assess not only individual, but also combined effects of increasing Fe and temperature as discussed
853 in the next section.

854

855 **4. 4 Enhanced responses to Fe with warming**

856 Fe addition led to an overall positive response of Chl *a* concentrations, phytoplankton photophysiology and
857 growth, but more so when combined with the ecologically relevant increase in temperature. The increase in
858 phytoplankton abundances was especially distinct for Weddell Sea bioassays. GLM analysis revealed that
859 temperature alone was a significant factor for total phytoplankton abundances, however more specifically, only
860 Phyto 3, Phyto 19 and Phyto 22 abundances displayed significant positive responses to temperature alone (T
861 treatment). The 2 °C warming alone was thus not a major driver of phytoplankton net growth in our bioassays,
862 but accelerated and enhanced Fe-addition responses (significant interaction effect for iron addition and
863 temperature increase on total phytoplankton abundances). The enhanced response to Fe with temperature was

864 especially distinct for bioassay W2 (average 1.61-fold change in total phytoplankton abundances in the TF
865 treatment compared to both F and T treatments; W1 showed a 1.48-fold average change). Despite low light levels,
866 this was also seen in Amundsen Sea bioassay A1, albeit to a lower extent (average 1.29-fold change in the TF
867 treatment compared to both F and T treatments). Larger-sized ($> 20 \mu\text{m}$) diatoms were mainly responsible for the
868 Chl *a* accumulation, which is consistent with previous studies (Noiri et al., 2005; Feng et al., 2010; Hinz et al.,
869 2012; Mills et al., 2012; Zhu et al., 2016) and supports the general consensus that especially large phytoplankton
870 show enhanced growth upon Fe addition due to their lower surface to volume ratio (Scharek et al., 1997). But also
871 (slightly) smaller diatoms Phyto 23 and 24 (average cell diameter of 15 and 19 μm , respectively) responded
872 positively to the combination of Fe and temperature. Diatom Phyto 24 was even the main phytoplankton
873 population responsible for the increase in the $< 20 \mu\text{m}$ Chl *a* fraction of the TF treatment in A1. The NMDS
874 analysis based on $< 20 \mu\text{m}$ phytoplankton abundances showed clustering for W1 and W2 driven by Fe addition
875 and temperature, indicating that also smaller-sized phytoplankton display positive responses. This is supported by
876 increased $< 20 \mu\text{m}$ Chl *a* concentrations and the 2.2 fold change in cellular carbon of $< 20 \mu\text{m}$ phytoplankton in
877 F and TF treatments in the Weddell Sea bioassays (compared to the C and T treatments). Specifically, we recorded
878 distinct abundance increases of the small 7 μm Phyto 16 and Phyto 17, in the F and TF treatments of W2.
879 *Phaeocystis antarctica* (Phyto 8; 3.7 μm) showed higher net growth rates for Fe-addition treatments in both
880 bioassay W1 and W2 but the effect was not very apparent and overall, *P. antarctica* seems to handle the other
881 treatments consistently well. Rose et al. (2009) and Zhu et al. (2016) also found diatoms preferentially stimulated
882 by Fe addition and/or temperature over *P. antarctica*, which was also found in a broader context where *P.*
883 *antarctica* dominated under Fe-low conditions, whilst diatoms dominated in regions with higher Fe concentrations
884 (Arrigo et al., 2017). In contrast, Andrew et al. (2019) found comparable growth rates for *P. antarctica* and several
885 diatom cultures (tested under Fe addition and warming treatments). Similar to our study, they found highest
886 growth for the combined Fe addition and warming treatment for most species. Since diatoms tended to increase
887 strongest with Fe addition, it can be speculated that phytoplankton community compositions shift towards more
888 diatoms with increases in Fe concentrations, however other biogeochemical factors are also important to consider.
889 The positive phytoplankton growth responses were population specific and Phyto 13 (5.5. μm) in W2 even showed
890 reduced abundances for the F and TF treatments, underscoring the multifaceted factors controlling phytoplankton
891 dynamics and emphasizing the importance of understanding how trace metal concentrations and climate change
892 together influence the marine ecosystems in the Southern Ocean.

893 Alterations in phytoplankton community composition and cell size, as observed in our experiments, will directly
894 affect top-down control by (microzooplankton) grazers and viral infection and consequently trophic transfer
895 efficiency (Eich et al. 2022, Biggs et al. 2021). Not only will the flow of organic carbon through the food web be
896 affected by the different phytoplankton mortality, also the flux of organic carbon to deeper layers of the ocean
897 (biological carbon pump) depends on the phytoplankton community composition, cell size and type of loss factor.
898 Since the seawater was not filtered before distribution to the cubitainers to reduce contamination risk, there is a
899 chance (although small, Voronina et al., 1994) that large grazers were introduced to the incubations. We did not
900 specifically sample for large grazers but did not notice any on the filters for Chl *a* and POC. Large grazers can be
901 expected to graze on larger phytoplankton (Hansen et al. 1994), thereby reducing phytoplankton net growth. This
902 would be most noticeable for the F and TF treatments, given the positive response of larger phytoplankton to Fe
903 addition. Our results would then be underestimating the effect of Fe enrichment. Moreover, grazing would likely
904 enhance with temperature (e.g., Lewandowska and Sommer, 2010; Karakuş et al., 2022), further reducing (and
905 underestimating) net growth rates of larger phytoplankton specifically in the TF treatment. Also,
906 microzooplankton grazing rates are known to increase with temperature (Chen et al., 2012; Caron & Hutchins,
907 2013), and even viral lysis may occur faster at higher temperature (Maat et al., 2017). This may partially explain
908 the small effect of warming in the bioassays. Besides temperature, Fe availability has been reported to affect algal
909 virus production and infectivity (Slagter et al., 2016; Kranzler et al., 2021). Changes observed in our experiments
910 might thus also have been affected by temperature and/or dFe related changes in loss factors affecting specific
911 phytoplankton groups.

912

913 **5. Conclusions**

914 Our study stands out in that it combined trace metal chemistry and biology, Chl *a*, and population abundance to
915 examine co-effects using natural Antarctic phytoplankton communities at environmentally realistic Fe
916 concentrations (+ 2 nM) and a predicted (2 °C) temperature increase (Boyd et al., 2015; Jabre et al., 2021; Andrew
917 et al., 2022). Bioassay incubations were performed under trace metal clean conditions (the entire duration) and
918 with temperature remaining stable over the course of incubations (maximum fluctuation of temperature ± 0.3 °C).
919 We stress the importance of trace metal clean working conditions to avoid inadvertently assigning Fe addition
920 effects on phytoplankton to temperature when working in low Fe regions (i.e. Southern Ocean, but also open
921 oceans in general). The differences we found between the F and TF treatment may have been assigned to
922 temperature alone under non-trace metal clean working conditions (as Fe would inadvertently have been

923 introduced), whilst our results show that temperature alone did not have a (major) effect. Our data also shows the
924 importance of considering other regional and/or seasonal factors potentially limiting phytoplankton growth, such
925 as e.g., light availability (limiting light conditions in bioassay A2) and dMn availability (potentially limiting in
926 W1), when studying the effect of future climate on Southern Ocean phytoplankton. Additionally, our data
927 indicates a trend of increased uptake of trace metals under dFe limitation, suggesting there are many adaptive
928 strategies employed by phytoplankton in navigating nutrient scarcities under varying environmental conditions,
929 with potential impact on the stoichiometry of global (micro-) nutrient distributions due to the central role of the
930 Southern Ocean. In general, the addition of Fe was the primary factor for observed stimulatory effects, with
931 temperature enhancing the effects of dFe. Especially large diatoms benefitted from Fe addition, although several
932 smaller-sized phytoplankton populations showed enhanced abundances upon Fe addition. Climate change is
933 predicted to lead to a shift towards smaller phytoplankton (Deppeler & Davidson, 2017; Krumhardt et al., 2022).
934 Our study shows, however, that enhanced Fe input counteracts this warming-induced shift, assuming
935 macronutrients will not become limiting. Given that the intensity of the observed effects varied between the
936 experiments with distinctly different phytoplankton communities, this study emphasizes the need for studying
937 diverse regions of the Southern Ocean and performing multiple bioassays over the productive season to better
938 understand and predict potential future changes, especially as future changes in Fe availability are region-specific
939 (Tagliabue et al., 2016; Van Manen et al., 2022). The Southern Ocean biogeochemical cycling and ecosystems
940 dynamics are complex and need to be better studied in field and modelling studies. The current study underlines
941 the need for assessing consequences of near future temperature changes at environmentally relevant dFe
942 concentrations.

943

944 *Data availability:* All data presented in this paper (nutrients, trace metals, phytoplankton abundances,
945 photosynthetic efficiencies, Chl *a* concentrations, pigment based community composition, particulate organic
946 carbon and particulate organic phosphate) are included in this published article and are available under
947 <https://doi.org/10.25850/nioz/7b.b.hh>.

948

949 *Supplement:* The supplementary material related to this article is available online at XXX.

950

951 *Author contributions:* RM and CPDB conceptualized the study. CE, MvM, EB, SBEHP, HT, IA, JSPM and RM
952 conducted the fieldwork under the lead of RM, JJ analysed the nutrient samples for Amundsen Sea bioassays,

953 WvdP analysed the pigment samples and conducted the Chemtax analysis, CE, MvM, wrote the original draft,
954 CPDB and RM edited the paper. EB, LJ and JSPM contributed to the discussion. All authors contributed to
955 commenting on the paper.

956

957 *Competing interests:* The authors declare that they have no conflict of interest.

958

959 *Acknowledgements:* We would like to thank the captain and crew of both the R/V Araon and the R/V Polarstern,
960 as well as the expedition leaders SangHoon Lee and Olaf Boebel and all other expedition participants. Our
961 participation in R/V Polarstern expedition PS117 was funded by AWI under grant number AWI_PS117_02.
962 Furthermore, we would like to thank John Seccombe from Aquahort for his support in conceiving and building
963 the heatpumps as well as his remote support during the expeditions and Sharyn Ossebaar for nutrient
964 measurements aboard R/V Polarstern. Sven Ober and all the colleagues from NIOZ national marine facilities
965 (NMF) for the preparation of the Titan sampling system during the expeditions, as well as building the incubators
966 and their help in the expedition preparation. We are also grateful to Bob Kusters (NIOZ) for his assistance with
967 the incubators, ensuring they maintained the correct temperature throughout our study. Patrick Laan (NIOZ) for
968 helping with the ICP-MS analyses, Flora Wille (NIOZ) for helping with the particulate metal analysis and Piet ter
969 Schure and his team (DMT Marine Equipment) for supplying a winch system last minute for the Titan sampling
970 system used on the R/V Araon.

971

972 *Financial support:* This work was part of the FePhyrus project (ALWPP.2016.020), which was supported by the
973 Netherlands Polar Programme (NPP), with financial aid from the Dutch Research Council (NWO). Mathijs van
974 Manen was supported by the Utrecht University-NIOZ collaboration. The ANA-08B expedition was supported
975 by the Korea Polar Research Institute grant KOPRI PE24110. The PS117 expedition was supported by the
976 auxiliary use proposal AWI_PS117_02. EMB was supported by an NSERC Canada Research Chair.

977 **References**

- 978 Aflenzer, H., Hoffmann, L., Holmes, T., Wuttig, K., Genovese, C., and Bowie, A. R.: Effect of dissolved iron (II) and
979 temperature on growth of the Southern Ocean phytoplankton species *Fragilariopsis cylindrus* and *Phaeocystis antarctica* ,
980 *Polar Biol*, 46, 1163–1173, <https://doi.org/10.1007/s00300-023-03191-z>, 2023.
- 981 Alderkamp, A.-C., Van Dijken, G.-L., Lowry, K. E., Connelly, T. L., Lagerström, M., Sherrell, R. M., Haskins, C.,
982 Rogalsky, E., Schofield, O., Stammerjohn, S. E., Yager, P. L., and Arrigo, K. R.: Fe availability drives phytoplankton
983 photosynthesis rates during spring bloom in the Amundsen Sea Polynya, Antarctica, *Elementa*, 3,
984 <https://doi.org/10.12952/journal.elementa.000043>, 2015.
- 985 Alderkamp, A.-C., Van Dijken, G. L., Lowry, K. E., Lewis, K. M., Joy-Warren, H. L., Van De Poll, W., Laan, P., Gerringa,
986 L., Delmont, T. O., Jenkins, B. D., and Arrigo, K. R.: Effects of iron and light availability on phytoplankton photosynthetic
987 properties in the Ross Sea, *Marine Ecology Progress Series*, 621, 33–50, <https://doi.org/10.3354/meps13000>, 2019.
- 988 Andrew, S. M., Morell, H. T., Strzepek, R. F., Boyd, P. W., and Ellwood, M. J.: Iron Availability Influences the Tolerance
989 of Southern Ocean Phytoplankton to Warming and Elevated Irradiance, *Frontiers in Marine Science*, 6, 2019.
- 990 Annett, A. L., Skiba, M., Henley, S. F., Venables, H. J., Meredith, M. P., Statham, P. J., and Ganeshram, R. S.: Comparative
991 roles of upwelling and glacial iron sources in Ryder Bay, coastal western Antarctic Peninsula, *Marine Chemistry*, 176, 21–
992 33, 2015.
- 993 Arrigo, K. R.: Marine microorganisms and global nutrient cycles, *Nature*, 437, 349–355,
994 <https://doi.org/10.1038/nature04159>, 2005.
- 995 Arrigo, K. R. and Van Dijken, G. L.: Phytoplankton dynamics within 37 Antarctic coastal polynya systems, *Journal of*
996 *Geophysical Research: Oceans*, 108, 2003.
- 997 Arrigo, K. R., Lowry, K. E., and van Dijken, G. L.: Annual changes in sea ice and phytoplankton in polynyas of the
998 Amundsen Sea, Antarctica, *Deep Sea Research Part II: Topical Studies in Oceanography*, 71, 5–15, 2012.
- 999 Arrigo, K. R., Van Dijken, G. L., Alderkamp, A., Erickson, Z. K., Lewis, K. M., Lowry, K. E., Joy-Warren, H. L., Middag,
1000 R., Nash-Arrigo, J. E., Selz, V., and Van De Poll, W.: Early Spring Phytoplankton Dynamics in the Western Antarctic
1001 Peninsula, *JGR Oceans*, 122, 9350–9369, <https://doi.org/10.1002/2017JC013281>, 2017.
- 1002 Assmy, P., Smetacek, V., Montresor, M., Klaas, C., Henjes, J., Strass, V. H., Arrieta, J. M., Bathmann, U., Berg, G. M., and
1003 Breitbarth, E.: Thick-shelled, grazer-protected diatoms decouple ocean carbon and silicon cycles in the iron-limited
1004 Antarctic Circumpolar Current, *Proceedings of the National Academy of Sciences*, 110, 20633–20638, 2013.
- 1005 de Baar, H. J., Buma, A. G., Nolting, R. F., Cadée, G. C., Jacques, G., and Tréguer, P. J.: On iron limitation of the Southern
1006 Ocean: experimental observations in the Weddell and Scotia Seas, *Marine ecology progress series*, 105–122, 1990.
- 1007 Balaguer, J., Koch, F., Hassler, C., and Trimborn, S.: Iron and manganese co-limit the growth of two phytoplankton groups
1008 dominant at two locations of the Drake Passage, *Communications Biology*, 5, 207, 2022.
- 1009 Balaguer, J., Thoms, S., and Trimborn, S.: The physiological response of an Antarctic key phytoplankton species to low iron
1010 and manganese concentrations, *Limnology & Oceanography*, 68, 2153–2166, <https://doi.org/10.1002/lno.12412>, 2023.
- 1011 Basterretxea, G., Font-Muñoz, J. S., Hernández-Carrasco, I., and Sañudo-Wilhelmy, S. A.: Global variability of high-
1012 nutrient low-chlorophyll regions using neural networks and wavelet coherence analysis, *Ocean Sci.*, 19, 973–990,
1013 <https://doi.org/10.5194/os-19-973-2023>, 2023.
- 1014 Bazzani, E., Lauritano, C., and Saggiomo, M.: Southern Ocean Iron Limitation of Primary Production between Past
1015 Knowledge and Future Projections, *Journal of Marine Science and Engineering*, 11, 272, 2023.
- 1016 Biggs, T. E., Alvarez-Fernandez, S., Evans, C., Mojica, K. D., Rozema, P. D., Venables, H. J., Pond, D. W., and Brussaard,
1017 C. P.: Antarctic phytoplankton community composition and size structure: importance of ice type and temperature as
1018 regulatory factors, *Polar Biology*, 42, 1997–2015, 2019.
- 1019 Biggs, T. E., Huisman, J., and Brussaard, C. P.: Viral lysis modifies seasonal phytoplankton dynamics and carbon flow in the
1020 Southern Ocean, *The ISME journal*, 15, 3615–3622, 2021.
- 1021 Boyd, P. W.: The role of iron in the biogeochemistry of the Southern Ocean and equatorial Pacific: a comparison of in situ
1022 iron enrichments, *Deep Sea Research Part II: Topical Studies in Oceanography*, 49, 1803–1821, 2002.

- 1023 Boyd, P. W., Arrigo, K. R., Strzepek, R., and Van Dijken, G. L.: Mapping phytoplankton iron utilization: Insights into
1024 Southern Ocean supply mechanisms, *Journal of Geophysical Research: Oceans*, 117, 2012.
- 1025 Boyd, P. W., Strzepek, R. F., Ellwood, M. J., Hutchins, D. A., Nodder, S. D., Twining, B. S., and Wilhelm, S. W.: Why are
1026 biotic iron pools uniform across high- and low-iron pelagic ecosystems?, *Global Biogeochemical Cycles*, 29, 1028–1043,
1027 <https://doi.org/10.1002/2014GB005014>, 2015.
- 1028 Bronselaer, B., Russell, J. L., Winton, M., Williams, N. L., Key, R. M., Dunne, J. P., Feely, R. A., Johnson, K. S., and
1029 Sarmiento, J. L.: Importance of wind and meltwater for observed chemical and physical changes in the Southern Ocean, *Nat.*
1030 *Geosci.*, 13, 35–42, <https://doi.org/10.1038/s41561-019-0502-8>, 2020.
- 1031 Browning, T. J., Achterberg, E. P., Engel, A., and Mawji, E.: Manganese co-limitation of phytoplankton growth and major
1032 nutrient drawdown in the Southern Ocean, *Nature communications*, 12, 884, 2021.
- 1033 Buesseler, K. O., Boyd, P. W., Black, E. E., and Siegel, D. A.: Metrics that matter for assessing the ocean biological carbon
1034 pump, *Proc. Natl. Acad. Sci. U.S.A.*, 117, 9679–9687, <https://doi.org/10.1073/pnas.1918114117>, 2020.
- 1035 Burns, S. M., Bundy, R. M., Abbott, W., Abdala, Z., Sterling, A. R., Chappell, P. D., Jenkins, B. D., and Buck, K. N.:
1036 Interactions of bioactive trace metals in shipboard Southern Ocean incubation experiments, *Limnology and Oceanography*,
1037 68, 525–543, <https://doi.org/10.1002/lno.12290>, 2023.
- 1038 Caron, D. A. and Hutchins, D. A.: The effects of changing climate on microzooplankton grazing and community structure:
1039 drivers, predictions and knowledge gaps, *Journal of Plankton Research*, 35, 235–252, <https://doi.org/10.1093/plankt/fbs091>,
1040 2013.
- 1041 Chen, B., Landry, M. R., Huang, B., and Liu, H.: Does warming enhance the effect of microzooplankton grazing on marine
1042 phytoplankton in the ocean?, *Limnology and oceanography*, 57, 519–526, 2012.
- 1043 Cullen, J. T., Chase, Z., Coale, K. H., Fitzwater, S. E., and Sherrell, R. M.: Effect of iron limitation on the cadmium to
1044 phosphorus ratio of natural phytoplankton assemblages from the Southern Ocean, *Limnology and Oceanography*, 48, 1079–
1045 1087, <https://doi.org/10.4319/lno.2003.48.3.1079>, 2003.
- 1046 Cunningham, B. R. and John, S. G.: The effect of iron limitation on cyanobacteria major nutrient and trace element
1047 stoichiometry, *Limnology and Oceanography*, 62, 846–858, <https://doi.org/10.1002/lno.10484>, 2017.
- 1048 Cutter, G., Casciotti, K., Croot, P., Geibert, W., Heimbürger, L.-E., Lohan, M., Planquette, H., and van de Flierdt, T.:
1049 Sampling and Sample-handling Protocols for GEOTRACES Cruises. Version 3, August 2017., 2017.
- 1050 Darelius, E., Daae, K., Dundas, V., Fer, I., Hellmer, H. H., Janout, M., Nicholls, K. W., Sallée, J.-B., and Østerhus, S.:
1051 Observational evidence for on-shelf heat transport driven by dense water export in the Weddell Sea, *Nature*
1052 *Communications*, 14, 1022, 2023.
- 1053 De Baar, H. J. W., Boyd, P. W., Coale, K. H., Landry, M. R., Tsuda, A., Assmy, P., Bakker, D. C. E., Bozec, Y., Barber, R.
1054 T., Brzezinski, M. A., Buesseler, K. O., Boyé, M., Croot, P. L., Gervais, F., Gorbunov, M. Y., Harrison, P. J., Hiscock, W.
1055 T., Laan, P., Lancelot, C., Law, C. S., Levasseur, M., Marchetti, A., Millero, F. J., Nishioka, J., Nojiri, Y., Van Oijen, T.,
1056 Riebesell, U., Rijkenberg, M. J. A., Saito, H., Takeda, S., Timmermans, K. R., Veldhuis, M. J. W., Waite, A. M., and Wong,
1057 C.: Synthesis of iron fertilization experiments: From the Iron Age in the Age of Enlightenment, *J. Geophys. Res.*, 110,
1058 2004JC002601, <https://doi.org/10.1029/2004JC002601>, 2005.
- 1059 De Baar, H. J. W., Timmermans, K. R., Laan, P., De Porto, H. H., Ober, S., Blom, J. J., Bakker, M. C., Schilling, J., Sarthou,
1060 G., and Smit, M. G.: Titan: A new facility for ultraclean sampling of trace elements and isotopes in the deep oceans in the
1061 international Geotraces program, *Marine Chemistry*, 111, 4–21, 2008.
- 1062 De Lavergne, C., Palter, J. B., Galbraith, E. D., Bernardello, R., and Marinov, I.: Cessation of deep convection in the open
1063 Southern Ocean under anthropogenic climate change, *Nature Climate Change*, 4, 278–282, 2014.
- 1064 Deppele, S. L. and Davidson, A. T.: Southern Ocean phytoplankton in a changing climate, *Frontiers in Marine Science*, 4,
1065 40, 2017.
- 1066 Drijfhout, S. S., Bull, C. Y. S., Hewitt, H., Holland, P. R., Jenkins, A., Mathiot, P., and Garabato, A. N.: An Amundsen Sea
1067 source of decadal temperature changes on the Antarctic continental shelf, *Ocean Dynamics*, 74, 37–52,
1068 <https://doi.org/10.1007/s10236-023-01587-3>, 2024.
- 1069 Eich, C., Pont, S. B., and Brussaard, C. P.: Effects of UV radiation on the chlorophyte *Micromonas polaris* host–virus

- 1070 interactions and MpoV-45T virus infectivity, *Microorganisms*, 9, 2429, 2021.
- 1071 Eich, C., Biggs, T. E., van de Poll, W. H., van Manen, M., Tian, H.-A., Jung, J., Lee, Y., Middag, R., and Brussaard, C. P.:
1072 Ecological importance of viral lysis as a loss factor of phytoplankton in the Amundsen Sea, *Microorganisms*, 10, 1967, 2022.
- 1073 Fahrbach, E., Hoppema, M., Rohardt, G., Schröder, M., and Wisotzki, A.: Decadal-scale variations of water mass properties
1074 in the deep Weddell Sea, *Ocean Dynamics*, 54, 77–91, 2004.
- 1075 Feng, Y., Hare, C. E., Rose, J. M., Handy, S. M., DiTullio, G. R., Lee, P. A., Smith Jr., W. O., Peloquin, J., Tozzi, S., Sun,
1076 J., Zhang, Y., Dunbar, R. B., Long, M. C., Sohst, B., Lohan, M., and Hutchins, D. A.: Interactive effects of iron, irradiance
1077 and CO₂ on Ross Sea phytoplankton, *Deep-Sea Research Part I: Oceanographic Research Papers*, 57, 368–383,
1078 <https://doi.org/10.1016/j.dsr.2009.10.013>, 2010.
- 1079 Fisher, B. J., Poulton, A. J., Meredith, M. P., Baldry, K., Schofield, O., and Henley, S. F.: Biogeochemistry of climate driven
1080 shifts in Southern Ocean primary producers, *Biogeosciences Discussions*, 1–29, 2023.
- 1081 Fourquez, M., Janssen, D. J., Conway, T. M., Cabanes, D., Ellwood, M. J., Sieber, M., Trimbom, S., and Hassler, C.:
1082 Chasing iron bioavailability in the Southern Ocean: Insights from *Phaeocystis antarctica* and iron speciation, *Sci. Adv.*, 9,
1083 eadf9696, <https://doi.org/10.1126/sciadv.adf9696>, 2023.
- 1084 Friedlingstein, P., O’sullivan, M., Jones, M. W., Andrew, R. M., Gregor, L., Hauck, J., Le Quéré, C., Luijkx, I. T., Olsen, A.,
1085 and Peters, G. P.: Global carbon budget 2022, *Earth System Science Data Discussions*, 2022, 1–159, 2022.
- 1086 Fukuda, R., Ogawa, H., Nagata, T., and Koike, I.: Direct Determination of Carbon and Nitrogen Contents of Natural
1087 Bacterial Assemblages in Marine Environments, *Appl Environ Microbiol*, 64, 3352–3358,
1088 <https://doi.org/10.1128/AEM.64.9.3352-3358.1998>, 1998.
- 1089 Garrison, D. L., Gowing, M. M., Hughes, M. P., Campbell, L., Caron, D. A., Dennett, M. R., Shalapyonok, A., Olson, R. J.,
1090 Landry, M. R., Brown, S. L., Liu, H.-B., Azam, F., Steward, G. F., Ducklow, H. W., and Smith, D. C.: Microbial food web
1091 structure in the Arabian Sea: a US JGOFS study, *Deep Sea Research Part II: Topical Studies in Oceanography*, 47, 1387–
1092 1422, [https://doi.org/10.1016/S0967-0645\(99\)00148-4](https://doi.org/10.1016/S0967-0645(99)00148-4), 2000.
- 1093 Geider, R. J.: Light and temperature dependence of the carbon to chlorophyll a ratio in microalgae and cyanobacteria:
1094 implications for physiology and growth of phytoplankton, *New Phytologist*, 1–34, 1987.
- 1095 Geider, R. J. and La Roche, J.: The role of iron in phytoplankton photosynthesis, and the potential for iron-limitation of
1096 primary productivity in the sea, *Photosynthesis research*, 39, 275–301, 1994.
- 1097 Gerringa, L. J., Alderkamp, A.-C., Laan, P., Thuroczy, C.-E., De Baar, H. J., Mills, M. M., van Dijken, G. L., van Haren, H.,
1098 and Arrigo, K. R.: Iron from melting glaciers fuels the phytoplankton blooms in Amundsen Sea (Southern Ocean): Iron
1099 biogeochemistry, *Deep Sea Research Part II: Topical Studies in Oceanography*, 71, 16–31, 2012.
- 1100 Gerringa, L. J. A., Alderkamp, A.-C., Laan, P., Thuróczy, C.-E., De Baar, H. J. W., Mills, M. M., van Dijken, G. L., van
1101 Haren, H., and Arrigo, K. R.: Corrigendum to "Iron from melting glaciers fuels the phytoplankton blooms in Amundsen Sea
1102 (Southern Ocean): iron biogeochemistry" (Gerringa et al., 2012), *Deep Sea Research Part II: Topical Studies in
1103 Oceanography*, 177, 104843, 2020.
- 1104 Gledhill, M. and Buck, K. N.: The organic complexation of iron in the marine environment: a review, *Frontiers in
1105 microbiology*, 3, 69, 2012.
- 1106 Gómez-Valdivia, F., Holland, P. R., Siahaan, A., Dutrieux, P., and Young, E.: Projected West Antarctic Ocean Warming
1107 Caused by an Expansion of the Ross Gyre, *Geophysical Research Letters*, 50, e2023GL102978,
1108 <https://doi.org/10.1029/2023GL102978>, 2023.
- 1109 Gordon, L. I., Jennings Jr, J. C., Ross, A. A., and Krest, J. M.: A suggested protocol for continuous flow automated analysis
1110 of seawater nutrients (phosphate, nitrate, nitrite and silicic acid) in the WOCE Hydrographic Program and the Joint Global
1111 Ocean Fluxes Study, *WOCE hydrographic program office, methods manual WHPO*, 1–52, 1993.
- 1112 Greene, R. M., Geider, R. J., Kolber, Z., and Falkowski, P. G.: Iron-Induced Changes in Light Harvesting and
1113 Photochemical Energy Conversion Processes in Eukaryotic Marine Algae I, *Plant Physiol*, 100, 565–575, 1992.
- 1114 Grise, K. M., Polvani, L. M., Tselioudis, G., Wu, Y., and Zelinka, M. D.: The ozone hole indirect effect: Cloud-radiative
1115 anomalies accompanying the poleward shift of the eddy-driven jet in the Southern Hemisphere, *Geophysical Research
1116 Letters*, 40, 3688–3692, <https://doi.org/10.1002/grl.50675>, 2013.

- 1117 van Haren, H., Brussaard, C. P., Gerringa, L. J., van Manen, M. H., Middag, R., and Groenewegen, R.: Diapycnal mixing
1118 across the photic zone of the NE-Atlantic, *Ocean Science Discussions*, 2020, 1–31, 2020.
- 1119 Hassler, C. S. and Schoemann, V.: Bioavailability of organically bound Fe to model phytoplankton of the Southern Ocean,
1120 *Biogeosciences*, 6, 2281–2296, 2009.
- 1121 Hawco, N. J., Tagliabue, A., and Twining, B. S.: Manganese Limitation of Phytoplankton Physiology and Productivity in the
1122 Southern Ocean, *Global Biogeochemical Cycles*, 36, e2022GB007382, <https://doi.org/10.1029/2022GB007382>, 2022.
- 1123 Hillenbrand, C.-D. and Cortese, G.: Polar stratification: A critical view from the Southern Ocean, *Palaeogeography*,
1124 *Palaeoclimatology, Palaeoecology*, 242, 240–252, 2006.
- 1125 Hinz, D. J., Nielsdóttir, M. C., Korb, R. E., Whitehouse, M. J., Poulton, A. J., Moore, C. M., Achterberg, E. P., and Bibby, T.
1126 S.: Responses of microplankton community structure to iron addition in the Scotia Sea, *Deep-Sea Research Part II: Topical*
1127 *Studies in Oceanography*, 59–60, 36–46, <https://doi.org/10.1016/j.dsr2.2011.08.006>, 2012.
- 1128 Hoppema, M., Middag, R., de Baar, H. J., Fahrbach, E., van Weerlee, E. M., and Thomas, H.: Whole season net community
1129 production in the Weddell Sea, *Polar Biology*, 31, 101–111, 2007.
- 1130 Hopwood, M. J., Carroll, D., Höfer, J., Achterberg, E. P., Meire, L., Le Moigne, F. A., Bach, L. T., Eich, C., Sutherland, D.
1131 A., and González, H. E.: Highly variable iron content modulates iceberg-ocean fertilisation and potential carbon export,
1132 *Nature Communications*, 10, 5261, 2019.
- 1133 Huang, Y., Fassbender, A. J., and Bushinsky, S. M.: Biogenic carbon pool production maintains the Southern Ocean carbon
1134 sink, *Proc. Natl. Acad. Sci. U.S.A.*, 120, e2217909120, <https://doi.org/10.1073/pnas.2217909120>, 2023.
- 1135 Hutchins, D. A. and Boyd, P. W.: Marine phytoplankton and the changing ocean iron cycle, *Nature Climate Change*, 6,
1136 1072–1079, 2016.
- 1137 Hutchins, D. A. and Bruland, K. W.: Iron-limited diatom growth and Si:N uptake ratios in a coastal upwelling regime,
1138 *Nature*, 393, 561–564, <https://doi.org/10.1038/31203>, 1998.
- 1139 Jabre, L. and Bertrand, E. M.: Interactive effects of iron and temperature on the growth of *Fragilariopsis cylindrus* ,
1140 *Limnology and Oceanography Letters*, 5, 363–370, 2020.
- 1141 Jabre, L. J., Allen, A. E., McCain, J. S. P., McCrow, J. P., Tenenbaum, N., Spackeen, J. L., Sipler, R. E., Green, B. R.,
1142 Bronk, D. A., Hutchins, D. A., and Bertrand, E. M.: Molecular underpinnings and biogeochemical consequences of
1143 enhanced diatom growth in a warming Southern Ocean, *Proceedings of the National Academy of Sciences*, 118,
1144 e2107238118, <https://doi.org/10.1073/pnas.2107238118>, 2021.
- 1145 Jensen, L. T., Wyatt, N. J., Landing, W. M., and Fitzsimmons, J. N.: Assessment of the stability, sorption, and
1146 exchangeability of marine dissolved and colloidal metals, *Marine Chemistry*, 220, 103754,
1147 <https://doi.org/10.1016/j.marchem.2020.103754>, 2020.
- 1148 Karakuş, O., Völker, C., Iversen, M., Hagen, W., and Hauck, J.: The Role of Zooplankton Grazing and Nutrient Recycling
1149 for Global Ocean Biogeochemistry and Phytoplankton Phenology, *JGR Biogeosciences*, 127, e2022JG006798,
1150 <https://doi.org/10.1029/2022JG006798>, 2022.
- 1151 Kelleher, M. K. and Grise, K. M.: Varied midlatitude shortwave cloud radiative responses to Southern Hemisphere
1152 circulation shifts, *Atmospheric Science Letters*, 23, e1068, <https://doi.org/10.1002/asl.1068>, 2022.
- 1153 Klunder, M. B., Laan, P., Middag, R., De Baar, H. J. W., and Van Ooijen, J. C.: Dissolved iron in the Southern Ocean
1154 (Atlantic sector), *Deep Sea Research Part II: Topical Studies in Oceanography*, 58, 2678–2694, 2011.
- 1155 Klunder, M. B., Laan, P., De Baar, H. J. W., Middag, R., Neven, I., and Van Ooijen, J.: Dissolved Fe across the Weddell Sea
1156 and Drake Passage: impact of DFe on nutrient uptake, *Biogeosciences*, 11, 651–669, 2014.
- 1157 Knust, R.: Polar research and supply vessel POLARSTERN operated by the Alfred-Wegener-Institute, *Journal of large-scale*
1158 *research facilities JLSRF*, 3, A119–A119, 2017.
- 1159 Kranzler, C. F., Brzezinski, M. A., Cohen, N. R., Lampe, R. H., Maniscalco, M., Till, C. P., Mack, J., Latham, J. R.,
1160 Bruland, K. W., and Twining, B. S.: Impaired viral infection and reduced mortality of diatoms in iron-limited oceanic
1161 regions, *Nature Geoscience*, 14, 231–237, 2021.

- 1162 Kroh, G. E. and Pilon, M.: Regulation of iron homeostasis and use in chloroplasts, *International Journal of Molecular*
1163 *Sciences*, 21, 3395, 2020.
- 1164 Krumhardt, K. M., Long, M. C., Sylvester, Z. T., and Petrik, C. M.: Climate drivers of Southern Ocean phytoplankton
1165 community composition and potential impacts on higher trophic levels, *Frontiers in Marine Science*, 9, 916140, 2022a.
- 1166 Krumhardt, K. M., Long, M. C., Sylvester, Z. T., and Petrik, C. M.: Climate drivers of Southern Ocean phytoplankton
1167 community composition and potential impacts on higher trophic levels, *Frontiers in Marine Science*, 9, 916140, 2022b.
- 1168 Kustka, A. B., Allen, A. E., and Morel, F. M.: Sequence analysis and transcriptional regulation of iron acquisition genes in
1169 two marine diatoms 1, *Journal of Phycology*, 43, 715–729, 2007.
- 1170 Lampe, R. H., Mann, E. L., Cohen, N. R., Till, C. P., Thamatrakoln, K., Brzezinski, M. A., Bruland, K. W., Twining, B. S.,
1171 and Marchetti, A.: Different iron storage strategies among bloom-forming diatoms, *Proceedings of the National Academy of*
1172 *Sciences*, 115, E12275–E12284, <https://doi.org/10.1073/pnas.1805243115>, 2018.
- 1173 Lane, E. S., Jang, K., Cullen, J. T., and Maldonado, M. T.: The interaction between inorganic iron and cadmium uptake in
1174 the marine diatom *Thalassiosira oceanica*, *Limnology and oceanography*, 53, 1784–1789, 2008.
- 1175 Lannuzel, D., Vancoppenolle, M., van Der Merwe, P., De Jong, J., Meiners, K. M., Grotti, M., Nishioka, J., and Schoemann,
1176 V.: Iron in sea ice: Review and new insights, *Elementa*, 4, 000130, 2016.
- 1177 Latour, P., Strzepek, R. F., Wuttig, K., van der Merwe, P., Bach, L. T., Eggins, S., Boyd, P. W., Ellwood, M. J., Pinfold, T.
1178 L., and Bowie, A. R.: Seasonality of phytoplankton growth limitation by iron and manganese in subantarctic waters,
1179 *Elementa: Science of the Anthropocene*, 11, 2023.
- 1180 Latour, P., Eggins, S., Van Der Merwe, P., Bach, L. T., Boyd, P. W., Ellwood, M. J., Bowie, A. R., Wuttig, K., and
1181 Strzepek, R. F.: Characterization of a Southern Ocean deep chlorophyll maximum: Response of phytoplankton to light, iron,
1182 and manganese enrichment, *Limnol Oceanogr Letters*, 9, 145–154, <https://doi.org/10.1002/lol2.10366>, 2024.
- 1183 Laufkötter, C., Vogt, M., Gruber, N., Aita-Noguchi, M., Aumont, O., Bopp, L., Buitenhuis, E., Doney, S. C., Dunne, J., and
1184 Hashioka, T.: Drivers and uncertainties of future global marine primary production in marine ecosystem models,
1185 *Biogeosciences*, 12, 6955–6984, 2015.
- 1186 Laws, E. A. and Bannister, T. T.: Nutrient-and light-limited growth of *Thalassiosira fluviatilis* in continuous culture, with
1187 implications for phytoplankton growth in the ocean 1, *Limnology and Oceanography*, 25, 457–473, 1980.
- 1188 Lewandowska, A. and Sommer, U.: Climate change and the spring bloom: a mesocosm study on the influence of light and
1189 temperature on phytoplankton and mesozooplankton, *Marine Ecology Progress Series*, 405, 101–111, 2010.
- 1190 Maat, D. S., Biggs, T., Evans, C., Van Bleijswijk, J. D. L., Van der Wel, N. N., Dutilh, B. E., and Brussaard, C. P. D.:
1191 Characterization and Temperature Dependence of Arctic *Micromonas polaris* Viruses, *Viruses*, 9, 134,
1192 <https://doi.org/10.3390/v9060134>, 2017.
- 1193 Mackey, M. D., Mackey, D. J., Higgins, H. W., and Wright, S. W.: CHEMTAX—a program for estimating class abundances
1194 from chemical markers: application to HPLC measurements of phytoplankton, *Marine Ecology Progress Series*, 144, 265–
1195 283, 1996.
- 1196 Marie, D., Partensky, F., Vaulot, D., and Brussaard, C.: Enumeration of Phytoplankton, Bacteria, and Viruses in Marine
1197 Samples, *CP Cytometry*, 10, <https://doi.org/10.1002/0471142956.cy1111s10>, 1999.
- 1198 Martin, J. H., Fitzwater, S. E., and Gordon, R. M.: Iron deficiency limits phytoplankton growth in Antarctic waters, *Global*
1199 *Biogeochemical Cycles*, 4, 5–12, 1990.
- 1200 McCain, J. S. P., Tagliabue, A., Susko, E., Achterberg, E. P., Allen, A. E., and Bertrand, E. M.: Cellular costs underpin
1201 micronutrient limitation in phytoplankton, *Science Advances*, 7, eabg6501, <https://doi.org/10.1126/sciadv.abg6501>, 2021.
- 1202 Meredith, M., M. Sommerkorn, S. Cassotta, C. Derksen, A. Ekaykin, A. Hollowed, G. Kofinas, A. Mackintosh, J.
1203 Melbourne-Thomas, M.M.C. Muelbert, G. Ottersen, H. Pritchard, and E.A.G. Schuur: Chapter 3: IPCC Polar regions —
1204 Special Report on the Ocean and Cryosphere in a Changing Climate, 2019.
- 1205 Meyerink, S. W., Ellwood, M. J., Maher, W. A., Dean Price, G., and Strzepek, R. F.: Effects of iron limitation on silicon
1206 uptake kinetics and elemental stoichiometry in two Southern Ocean diatoms, *Eucampia antarctica* and *Proboscia inermis* ,
1207 and the temperate diatom *Thalassiosira pseudonana*, *Limnology & Oceanography*, 62, 2445–2462,

- 1208 <https://doi.org/10.1002/lno.10578>, 2017.
- 1209 Middag, R., De Baar, H. J., Bruland, K. W., and Van Heuven, S. M.: The distribution of nickel in the West-Atlantic Ocean,
1210 its relationship with phosphate and a comparison to cadmium and zinc, *Frontiers in Marine Science*, 7, 105, 2020.
- 1211 Middag, R., Zitoun, R., and Conway, T.: Trace Metals, in: *Marine Analytical Chemistry*, edited by: Blasco, J. and Tovar-
1212 Sánchez, A., Springer International Publishing, Cham, 103–198, https://doi.org/10.1007/978-3-031-14486-8_3, 2023.
- 1213 Millero, F. J., Sotolongo, S., and Izaguirre, M.: The oxidation kinetics of Fe (II) in seawater, *Geochimica et Cosmochimica*
1214 *Acta*, 51, 793–801, 1987.
- 1215 Milligan, A. J. and Harrison, P. J.: Effects of non-steady-state iron limitation on nitrogen assimilatory enzymes in the marine
1216 diatom *thalassiosira weissflogii* (BACILLARIOPHYCEAE), *Journal of Phycology*, 36, 78–86,
1217 <https://doi.org/10.1046/j.1529-8817.2000.99013.x>, 2000.
- 1218 Mills, M. M., Alderkamp, A.-C., Thuróczy, C.-E., van Dijken, G. L., Laan, P., de Baar, H. J., and Arrigo, K. R.:
1219 Phytoplankton biomass and pigment responses to Fe amendments in the Pine Island and Amundsen polynyas, *Deep Sea*
1220 *Research Part II: Topical Studies in Oceanography*, 71, 61–76, 2012.
- 1221 Minas, H. J. and Minas, M.: Net community production in High nutrient-low chlorophyll waters of the tropical and Antarctic
1222 oceans-grazing vs iron hypothesis, *Oceanologica Acta*, 15, 145–162, 1992.
- 1223 Misumi, K., Lindsay, K., Bryan, F. O., Moore, J. K., Doney, S. C., Tsumune, D., and Yoshida, Y.: The iron budget in ocean
1224 surface waters in the 20th and 21st centuries: Projections by the Community Earth System Model version 1, *Biogeosci.*
1225 *Discuss*, 10, 8505–8559, 2013.
- 1226 Moore, C. M., Seeyave, S., Hickman, A. E., Allen, J. T., Lucas, M. I., Planquette, H., Pollard, R. T., and Poulton, A. J.: Iron-
1227 light interactions during the CROZet natural iron bloom and EXport experiment (CROZEX) I: Phytoplankton growth and
1228 photophysiology, *Deep-Sea Research Part II: Topical Studies in Oceanography*, 54, 2045–2065,
1229 <https://doi.org/10.1016/j.dsr2.2007.06.011>, 2007.
- 1230 Moore, C. M., Mills, M. M., Arrigo, K. R., Berman-Frank, I., Bopp, L., Boyd, P. W., Galbraith, E. D., Geider, R. J., Guieu,
1231 C., Jaccard, S. L., Jickells, T. D., La Roche, J., Lenton, T. M., Mahowald, N. M., Marañón, E., Marinov, I., Moore, J. K.,
1232 Nakatsuka, T., Oschlies, A., Saito, M. A., Thingstad, T. F., Tsuda, A., and Ulloa, O.: Processes and patterns of oceanic
1233 nutrient limitation, *Nature Geosci*, 6, 701–710, <https://doi.org/10.1038/ngeo1765>, 2013.
- 1234 Moore, J. K., Fu, W., Primeau, F., Britten, G. L., Lindsay, K., Long, M., Doney, S. C., Mahowald, N., Hoffman, F., and
1235 Randerson, J. T.: Sustained climate warming drives declining marine biological productivity, *Science*, 359, 1139–1143,
1236 <https://doi.org/10.1126/science.aa06379>, 2018.
- 1237 Morán, X. A. G., Sebastián, M., Pedrís-Alí, C., and Estrada, M.: Response of Southern Ocean phytoplankton and
1238 bacterioplankton production to short-term experimental warming, *Limnology & Oceanography*, 51, 1791–1800,
1239 <https://doi.org/10.4319/lo.2006.51.4.1791>, 2006.
- 1240 Moreau, S., Hattermann, T., de Steur, L., Kauko, H. M., Ahonen, H., Ardelan, M., Assmy, P., Chierici, M., Descamps, S.,
1241 Dinter, T., Falkenhaus, T., Fransson, A., Grønningsæter, E., Hallfredsson, E. H., Huhn, O., Lebrun, A., Lowther, A.,
1242 Lübcker, N., Monteiro, P., Peeken, I., Roychoudhury, A., Róžańska, M., Ryan-Keogh, T., Sanchez, N., Singh, A., Simonsen,
1243 J. H., Steiger, N., Thomalla, S. J., van Tonder, A., Wiktor, J. M., and Steen, H.: Wind-driven upwelling of iron sustains
1244 dense blooms and food webs in the eastern Weddell Gyre, *Nat Commun*, 14, 1303, <https://doi.org/10.1038/s41467-023-36992-1>, 2023.
- 1246 Noiri, Y., Kudo, I., Kiyosawa, H., Nishioka, J., and Tsuda, A.: Influence of iron and temperature on growth, nutrient
1247 utilization ratios and phytoplankton species composition in the western subarctic Pacific Ocean during the SEEDS
1248 experiment, *Progress in Oceanography*, 64, 149–166, 2005.
- 1249 Ohnemus, D. C., Auro, M. E., Sherrell, R. M., Lagerström, M., Morton, P. L., Twining, B. S., Rauschenberg, S., and Lam, P.
1250 J.: Laboratory intercomparison of marine particulate digestions including Piranha: a novel chemical method for dissolution
1251 of polyethersulfone filters, *Limnology & Ocean Methods*, 12, 530–547, <https://doi.org/10.4319/lom.2014.12.530>, 2014.
- 1252 Olson, R. J., Sosik, H. M., Chekalyuk, A. M., and Shalapyonok, A.: Effects of iron enrichment on phytoplankton in the
1253 Southern Ocean during late summer: Active fluorescence and flow cytometric analyses, *Deep-Sea Research Part II: Topical*
1254 *Studies in Oceanography*, 47, 3181–3200, [https://doi.org/10.1016/S0967-0645\(00\)00064-3](https://doi.org/10.1016/S0967-0645(00)00064-3), 2000.
- 1255 Park, J., Kuzminov, F. I., Bailleul, B., Yang, E. J., Lee, S., Falkowski, P. G., and Gorbunov, M. Y.: Light availability rather
1256 than Fe controls the magnitude of massive phytoplankton bloom in the Amundsen Sea polynyas, *Antarctica, Limnology and*

- 1257 Oceanography, 62, 2260–2276, <https://doi.org/10.1002/lno.10565>, 2017.
- 1258 Pausch, F., Bischof, K., and Trimborn, S.: Iron and manganese co-limit growth of the Southern Ocean diatom *Chaetoceros*
1259 *debilis*, PLOS ONE, 14, e0221959, <https://doi.org/10.1371/journal.pone.0221959>, 2019.
- 1260 Peers, G. and Price, N. M.: A role for manganese in superoxide dismutases and growth of iron-deficient diatoms, *Limnology*
1261 *& Oceanography*, 49, 1774–1783, <https://doi.org/10.4319/lo.2004.49.5.1774>, 2004.
- 1262 Petrou, K., Kranz, S. A., Trimborn, S., Hassler, C. S., Ameijeiras, S. B., Sackett, O., Ralph, P. J., and Davidson, A. T.:
1263 Southern Ocean phytoplankton physiology in a changing climate, *Journal of Plant Physiology*, 203, 135–150, 2016.
- 1264 Pinkerton, M. H., Boyd, P. W., Deppeler, S., Hayward, A., Höfer, J., and Moreau, S.: Evidence for the impact of climate
1265 change on primary producers in the Southern Ocean, *Frontiers in Ecology and Evolution*, 9, 592027, 2021.
- 1266 Planquette, H. and Sherrell, R. M.: Sampling for particulate trace element determination using water sampling bottles:
1267 methodology and comparison to in situ pumps, *Limnology and Oceanography: Methods*, 10, 367–388, 2012.
- 1268 Primeau, F. W., Holzer, M., and DeVries, T.: Southern Ocean nutrient trapping and the efficiency of the biological pump, *J.*
1269 *Geophys. Res. Oceans*, 118, 2547–2564, <https://doi.org/10.1002/jgrc.20181>, 2013.
- 1270 Raiswell, R., Benning, L. G., Tranter, M., and Tulaczyk, S.: Bioavailable iron in the Southern Ocean: the significance of the
1271 iceberg conveyor belt, *Geochem Trans*, 9, 7, <https://doi.org/10.1186/1467-4866-9-7>, 2008.
- 1272 Raiswell, R., Hawkings, J. R., Benning, L. G., Baker, A. R., Death, R., Albani, S., Mahowald, N., Krom, M. D., Poulton, S.
1273 W., and Wadham, J.: Potentially bioavailable iron delivery by iceberg-hosted sediments and atmospheric dust to the polar
1274 oceans, *Biogeosciences*, 13, 3887–3900, 2016.
- 1275 Raven, J. A.: Predictions of Mn and Fe use efficiencies of phototrophic growth as a function of light availability for growth
1276 and of C assimilation pathway, *New Phytologist*, 116, 1–18, <https://doi.org/10.1111/j.1469-8137.1990.tb00505.x>, 1990.
- 1277 Reay, D. S., Priddle, J., Nedwell, D. B., Whitehouse, M. J., Ellis-Evans, J. C., Deubert, C., and Connelly, D. P.: Regulation
1278 by low temperature of phytoplankton growth and nutrient uptake in the Southern Ocean, *Marine Ecology Progress Series*,
1279 219, 51–64, 2001.
- 1280 Rignot, E., Jacobs, S., Mouginot, J., and Scheuchl, B.: Ice-Shelf Melting Around Antarctica, *Science*, 341, 266–270,
1281 <https://doi.org/10.1126/science.1235798>, 2013.
- 1282 Rijkenberg, M. J., de Baar, H. J., Bakker, K., Gerringa, L. J., Keijzer, E., Laan, M., Laan, P., Middag, R., Ober, S., and van
1283 Ooijen, J.: “PRISTINE”, a new high volume sampler for ultraclean sampling of trace metals and isotopes, *Marine*
1284 *Chemistry*, 177, 501–509, 2015.
- 1285 Rose, J. M., Feng, Y., DiTullio, G. R., Dunbar, R. B., Hare, C. E., Lee, P. A., Lohan, M., Long, M., Smith Jr, W. O., and
1286 Sohst, B.: Synergistic effects of iron and temperature on Antarctic phytoplankton and microzooplankton assemblages,
1287 *Biogeosciences*, 6, 3131–3147, 2009.
- 1288 Ryan-Keogh, T. J., Thomalla, S. J., Monteiro, P. M., and Tagliabue, A.: Multidecadal trend of increasing iron stress in
1289 Southern Ocean phytoplankton, *Science*, 379, 834–840, 2023.
- 1290 Ryderheim, F., Grønning, J., and Kiørboe, T.: Thicker shells reduce copepod grazing on diatoms, *Limnology and*
1291 *Oceanography Letters*, 7, 435–442, 2022.
- 1292 Sarmiento, J. L., Gruber, N., Brzezinski, M. A., and Dunne, J. P.: High-latitude controls of thermocline nutrients and low
1293 latitude biological productivity, *Nature*, 427, 56–60, <https://doi.org/10.1038/nature02127>, 2004.
- 1294 Schoffman, H., Lis, H., Shaked, Y., and Keren, N.: Iron–Nutrient Interactions within Phytoplankton, *Frontiers in Plant*
1295 *Science*, 7, 2016.
- 1296 Schofield, O., Miles, T., Alderkamp, A.-C., Lee, S., Haskins, C., Rogalsky, E., Sipler, R., Sherrell, R. M., and Yager, P. L.:
1297 In situ phytoplankton distributions in the Amundsen Sea Polynya measured by autonomous gliders, *Elementa*, 3, 000073,
1298 2015.
- 1299 Selz, V., Lowry, K. E., Lewis, K. M., Joy-Warren, H. L., van de Poll, W., Nirmel, S., Tong, A., and Arrigo, K. R.:
1300 Distribution of *Phaeocystis antarctica*-dominated sea ice algal communities and their potential to seed phytoplankton across
1301 the western Antarctic Peninsula in spring, *Marine Ecology Progress Series*, 586, 91–112, 2018.

- 1302 Seyitmuhammedov, K., Stirling, C. H., Reid, M. R., van Hale, R., Laan, P., Arrigo, K. R., van Dijken, G., Alderkamp, A.-C.,
1303 and Middag, R.: The distribution of Fe across the shelf of the Western Antarctic Peninsula at the start of the phytoplankton
1304 growing season, *Marine Chemistry*, 238, 104066, 2022.
- 1305 Shaw, T. J., Smith Jr, K. L., Hexel, C. R., Dudgeon, R., Sherman, A. D., Vernet, M., and Kaufmann, R. S.: ²³⁴Th-based
1306 carbon export around free-drifting icebergs in the Southern Ocean, *Deep Sea Research Part II: Topical Studies in*
1307 *Oceanography*, 58, 1384–1391, 2011.
- 1308 Sherrell, R. M., Lagerström, M. E., Forsch, K. O., Stammerjohn, S. E., and Yager, P. L.: Dynamics of dissolved iron and
1309 other bioactive trace metals (Mn, Ni, Cu, Zn) in the Amundsen Sea Polynya, Antarctica, *Elementa: Science of the*
1310 *Anthropocene*, 3, 000071, <https://doi.org/10.12952/journal.elementa.000071>, 2015.
- 1311 Shi, J.-R., Talley, L. D., Xie, S.-P., Liu, W., and Gille, S. T.: Effects of buoyancy and wind forcing on Southern Ocean
1312 climate change, *Journal of Climate*, 33, 10003–10020, 2020.
- 1313 Sieber, M., Conway, T. M., de Souza, G. F., Hassler, C. S., Ellwood, M. J., and Vance, D.: Isotopic fingerprinting of
1314 biogeochemical processes and iron sources in the iron-limited surface Southern Ocean, *Earth and Planetary Science Letters*,
1315 567, 116967, 2021.
- 1316 Sinha, A. K., Parli Venkateswaran, B., Tripathy, S. C., Sarkar, A., and Prabhakaran, S.: Effects of growth conditions on
1317 siderophore producing bacteria and siderophore production from Indian Ocean sector of Southern Ocean, *J Basic Microbiol*,
1318 59, 412–424, <https://doi.org/10.1002/jobm.201800537>, 2019.
- 1319 Slagter, H. A., Gerringa, L. J. A., and Brussaard, C. P. D.: Phytoplankton Virus Production Negatively Affected by Iron
1320 Limitation, *Frontiers in Marine Science*, 3, 2016.
- 1321 Stapleford, L. S. and Smith, R. E.: The interactive effects of temperature and silicon limitation on the psychrophilic ice
1322 diatom *Pseudonitzschia seriata*, *Polar Biology*, 16, 589–594, 1996.
- 1323 Strass, V. H., Rohardt, G., Kanzow, T., Hoppema, M., and Boebel, O.: Multidecadal Warming and Density Loss in the Deep
1324 Weddell Sea, Antarctica, *Journal of Climate*, 33, 9863–9881, <https://doi.org/10.1175/JCLI-D-20-0271.1>, 2020.
- 1325 Strzepek, R. F., Boyd, P. W., and Sunda, W. G.: Photosynthetic adaptation to low iron, light, and temperature in Southern
1326 Ocean phytoplankton, *Proceedings of the National Academy of Sciences*, 116, 4388–4393, 2019.
- 1327 Tagliabue, A., Aumont, O., DeAth, R., Dunne, J. P., Dutkiewicz, S., Galbraith, E., Misumi, K., Moore, J. K., Ridgwell, A.,
1328 Sherman, E., Stock, C., Vichi, M., Völker, C., and Yool, A.: How well do global ocean biogeochemistry models simulate
1329 dissolved iron distributions?, *Global Biogeochemical Cycles*, 30, 149–174, <https://doi.org/10.1002/2015GB005289>, 2016.
- 1330 Takahashi, T., Sweeney, C., Hales, B., Chipman, D. W., Newberger, T., Goddard, J. G., Iannuzzi, R. A., and Sutherland, S.
1331 C.: The changing carbon cycle in the Southern Ocean, *Oceanography*, 25, 26–37, 2012.
- 1332 Taylor, S. R. and McLennan, S. M.: *The continental crust: its composition and evolution*, 1985.
- 1333 Teske, V., Timmermann, R., and Semmler, T.: Subsurface warming in the Antarctica’s Weddell Sea can be avoided by
1334 reaching the 2°C warming target, *Communications Earth & Environment*, 5, 93, 2024.
- 1335 Thomalla, S. J., Nicholson, S.-A., Ryan-Keogh, T. J., and Smith, M. E.: Widespread changes in Southern Ocean
1336 phytoplankton blooms linked to climate drivers, *Nature Climate Change*, 13, 975–984, 2023.
- 1337 Turner, J., Colwell, S. R., Marshall, G. J., Lachlan-Cope, T. A., Carleton, A. M., Jones, P. D., Lagun, V., Reid, P. A., and
1338 Iagovkina, S.: Antarctic climate change during the last 50 years, *International journal of Climatology*, 25, 279–294, 2005.
- 1339 Twining, B. S. and Baines, S. B.: The trace metal composition of marine phytoplankton, *Annual review of marine science*, 5,
1340 191–215, 2013.
- 1341 Twining, B. S., Baines, S. B., and Fisher, N. S.: Element stoichiometries of individual plankton cells collected during the
1342 Southern Ocean Iron Experiment (SOFEX), *Limnology and oceanography*, 49, 2115–2128, 2004.
- 1343 Van der Merwe, P., Wuttig, K., Holmes, T., Trull, T. W., Chase, Z., Townsend, A. T., Goemann, K., and Bowie, A. R.: High
1344 lability Fe particles sourced from glacial erosion can meet previously unaccounted biological demand: Heard Island,
1345 Southern Ocean, *Frontiers in Marine Science*, 6, 332, 2019.
- 1346 Van Heukelem, L. and Thomas, C. S.: Computer-assisted high-performance liquid chromatography method development

- 1347 with applications to the isolation and analysis of phytoplankton pigments, *Journal of Chromatography A*, 910, 31–49, 2001.
- 1348 Van Leeuwe, M. A., Villerius, L. A., Roggeveld, J., Visser, R. J. W., and Stefels, J.: An optimized method for automated
1349 analysis of algal pigments by HPLC, *Marine chemistry*, 102, 267–275, 2006.
- 1350 Van Manen, M., Aoki, S., Brussaard, C. P., Conway, T. M., Eich, C., Gerringa, L. J., Jung, J., Kim, T.-W., Lee, S., and Lee,
1351 Y.: The role of the Dotson Ice Shelf and Circumpolar Deep Water as driver and source of dissolved and particulate iron and
1352 manganese in the Amundsen Sea polynya, *Southern Ocean, Marine Chemistry*, 246, 104161, 2022.
- 1353 Van Oijen, T., Van Leeuwe, M. A., Granum, E., Weissing, F. J., Bellerby, R. G. J., Gieskes, W. W. C., and De Baar, H. J.
1354 W.: Light rather than iron controls photosynthate production and allocation in Southern Ocean phytoplankton populations
1355 during austral autumn, *Journal of Plankton Research*, 26, 885–900, 2004.
- 1356 Veldhuis, M. J. and Kraay, G. W.: Phytoplankton in the subtropical Atlantic Ocean: towards a better assessment of biomass
1357 and composition, *Deep Sea Research Part I: Oceanographic Research Papers*, 51, 507–530, 2004.
- 1358 Venables, H. and Moore, C. M.: Phytoplankton and light limitation in the Southern Ocean: Learning from high-nutrient,
1359 high-chlorophyll areas, *Journal of Geophysical Research: Oceans*, 115, <https://doi.org/10.1029/2009JC005361>, 2010.
- 1360 Verardo, D. J., Froelich, P. N., and McIntyre, A.: Determination of organic carbon and nitrogen in marine sediments using
1361 the Carlo Erba NA-1500 Analyzer, *Deep Sea Research Part A. Oceanographic Research Papers*, 37, 157–165, 1990.
- 1362 Viljoen, J. J., Philibert, R., Van Horsten, N., Mtshali, T., Roychoudhury, A. N., Thomalla, S., and Fietz, S.: Phytoplankton
1363 response in growth, photophysiology and community structure to iron and light in the Polar Frontal Zone and Antarctic
1364 waters, *Deep-Sea Research Part I: Oceanographic Research Papers*, 141, 118–129, <https://doi.org/10.1016/j.dsr.2018.09.006>,
1365 2018.
- 1366 Vives, C. R., Schallenberg, C., Strutton, P. G., and Westwood, K. J.: Iron and light limitation of phytoplankton growth off
1367 East Antarctica, *Journal of Marine Systems*, 234, <https://doi.org/10.1016/j.jmarsys.2022.103774>, 2022.
- 1368 Von Berg, L., Prend, C. J., Campbell, E. C., Mazloff, M. R., Talley, L. D., and Gille, S. T.: Weddell Sea Phytoplankton
1369 Blooms Modulated by Sea Ice Variability and Polynya Formation, *Geophysical Research Letters*, 47, e2020GL087954,
1370 <https://doi.org/10.1029/2020GL087954>, 2020.
- 1371 Voronina, N. M., Kosobokova, K. N., and Pakhomov, E. A.: Composition and biomass of summer metazoan plankton in the
1372 0-200 m layer of the Atlantic sector of the Antarctic, *Polar Biol*, 14, <https://doi.org/10.1007/BF00234970>, 1994.
- 1373 Waite, A. M. and Nodder, S. D.: The effect of in situ iron addition on the sinking rates and export flux of Southern Ocean
1374 diatoms, *Deep Sea Research Part II: Topical Studies in Oceanography*, 48, 2635–2654, 2001.
- 1375 Wang, X. J., Behrenfeld, M., Le Borgne, R., Murtugudde, R., and Boss, E.: Regulation of phytoplankton carbon to
1376 chlorophyll ratio by light, nutrients and temperature in the Equatorial Pacific Ocean: a basin-scale model, *Biogeosciences*, 6,
1377 391–404, 2009.
- 1378 Wolfe-Simon, F., Grzebyk, D., Schofield, O., and Falkowski, P. G.: The role and evolution of superoxide dismutases in
1379 algae, *Journal of Phycology*, 41, 453–465, <https://doi.org/10.1111/j.1529-8817.2005.00086.x>, 2005.
- 1380 Worden, A. Z., Nolan, J. K., and Palenik, B.: Assessing the dynamics and ecology of marine picophytoplankton: The
1381 importance of the eukaryotic component, *Limnology and Oceanography*, 49, 168–179,
1382 <https://doi.org/10.4319/lo.2004.49.1.0168>, 2004.
- 1383 Wu, M., McCain, J. S. P., Rowland, E., Middag, R., Sandgren, M., Allen, A. E., and Bertrand, E. M.: Manganese and iron
1384 deficiency in Southern Ocean *Phaeocystis antarctica* populations revealed through taxon-specific protein indicators, *Nature*
1385 *Communications*, 10, 3582, <https://doi.org/10.1038/s41467-019-11426-z>, 2019.
- 1386 Yoon, J.-E., Yoo, K.-C., Macdonald, A. M., Yoon, H.-I., Park, K.-T., Yang, E. J., Kim, H.-C., Lee, J. I., Lee, M. K., Jung, J.,
1387 Park, J., Lee, J., Kim, S., Kim, S.-S., Kim, K., and Kim, I.-N.: Reviews and syntheses: Ocean iron fertilization experiments –
1388 past, present, and future looking to a future Korean Iron Fertilization Experiment in the Southern Ocean (KIFES) project,
1389 *Biogeosciences*, 15, 5847–5889, <https://doi.org/10.5194/bg-15-5847-2018>, 2018.
- 1390 Zhu, Z., Xu, K., Fu, F., Spackeen, J. L., Bronk, D. A., and Hutchins, D. A.: A comparative study of iron and temperature
1391 interactive effects on diatoms and *Phaeocystis antarctica* from the Ross Sea, Antarctica, *Marine Ecology Progress Series*,
1392 550, 39–51, 2016.

